

IceCube expectations for two high-energy neutrino production models at active galactic nuclei

C.A. Argüelles,^{1,*} M. Bustamante,^{1,2,†} and A.M. Gago^{1,‡}

¹*Sección Física, Departamento de Ciencias, Pontificia Universidad Católica del Perú, Apartado 1761, Lima, Perú*

²*Theoretical Physics Department, Fermi National Accelerator Laboratory, Batavia, IL 60510, USA*

(Dated: June 1, 2019)

We have determined the current and near-future allowed regions of the parameter spaces of two representative models of diffuse neutrino flux from active galactic nuclei (AGN): one by Koers & Tinyakov (KT), which assumes that the neutrino production occurs in a region close to the source, and another by Becker & Biermann (BB), which considers that it occurs inside the AGN jets. With this aim, we have used as observable the predicted number of downgoing and upgoing muon-neutrinos at the IceCube detector, after five years of exposure, in the energy range $10^5 \leq E_\nu/\text{GeV} \leq 10^8$. The lower boundary of these allowed regions has been fixed by the projected sensitivity of the completed IceCube neutrino detector, while for the upper boundary we have used either the reported upper bound on the neutrino flux by the AMANDA experiment or a projected, tighter, upper bound, found by assuming that no signal is present in the data that has been recorded by the half-completed IceCube array (IC40). For the analysis, we have varied the spectral index α of the power-law fluxes $\propto E_\nu^{-\alpha}$ proposed by the KT and BB models, plus two additional parameters of the BB model, the ratio between the boost factors of neutrinos and cosmic rays, $\Gamma_\nu/\Gamma_{\text{CR}}$, and the maximum redshift, $z_{\text{CR}}^{\text{max}}$, up to which a source can contribute to the diffuse neutrino flux. Additionally, for the KT model, we have considered a scenario in which the number density of sources does not evolve with redshift and one in which it evolves strongly, following the star formation rate. We have found that, if we consider 2.7 to be the true value of the spectral index, the strong source evolution case for the KT model is excluded by the IC40 bound, while the case of no source evolution is allowed by it, with values of α ranging up to 2.88. The AMANDA bound allows both cases of the KT model, with α going up to 3.04(2.8) for no (strong) source evolution. For the BB model, $\alpha = 2.7$ is allowed only within a very narrow region, with $\Gamma_\nu/\Gamma_{\text{CR}} \lesssim 2$ and $z_{\text{CR}}^{\text{max}} \approx 0.03$, regardless of the upper bound used. Also, with 2.7 as a benchmark, it is observed that values of $\Gamma_\nu/\Gamma_{\text{CR}} \geq 10$ are not allowed. Finally, we have analysed the capacity of IceCube to discriminate between the two models within the parameter regions where they are simultaneously allowed. We have found that the separation between models is less than 5σ only inside a small region, where $\Gamma_\nu/\Gamma_{\text{CR}}$ and α are contained within 1.2(4.5)–2.2(7) and 2.55(2.15)–2.68(2.3), respectively, with $z_{\text{CR}}^{\text{max}}$ between 0.01 and 0.03, and for the case of no (strong) source evolution. Outside this region, the predictions from the models can be clearly separated.

PACS numbers: 95.85.Ry

Keywords: AGN neutrino, Auger, cosmic ray, UHECR, astrophysical neutrino

I. INTRODUCTION

Active Galactic Nuclei (AGN) are the most luminous persistent objects in the Universe, emitting radiation along almost the entire electromagnetic spectrum, with typical luminosities on the order of $10^{42} \text{ erg s}^{-1}$ (see, e.g., [1, 2]). There is evidence that supports the idea that AGN are powered by matter accreting onto a central supermassive black hole, with a mass between 10^6 and 10^{10} times the solar mass [3, 4]. In some cases an enormous amount of energy is released in the form of two highly-collimated relativistic jets that emerge in opposite directions, perpendicularly to the accretion disc. Although the composition of these jets is unknown, it is widely believed that they contain high-energy charged particles, such as electrons, protons and ionised nuclei, which have been accelerated as a result of the repeated crossings of the shock fronts that exist within gas clouds moving at relativistic speeds along the jets. Such a process would be able to give protons and nuclei energies of up to $\sim 10^{20} \text{ eV}$ [5, 6].

Recently, the Pierre Auger Observatory (PAO) claimed to have detected 27 cosmic-ray events with energies above 57 EeV [7], providing evidence of the anisotropy in the arrival directions of ultrahigh-energy cosmic rays (UHECRs).

*Electronic address: c.arguelles@pucp.edu.pe

†Electronic address: mbustamante@pucp.edu.pe

‡Electronic address: agago@pucp.edu.pe

Based on the observation of 20 of these events having an angular separation equal to or less than 3.2° from the positions of AGN from the 12th edition Véron-Cetty & Véron catalogue [8], a possible correlation was found with AGN lying relatively close, at distances of 75 Mpc or less. Even though the claim on the correlation has since lost some ground [9, 10], it still constitutes a possible hint towards identifying AGN as the sources of the highest-energy cosmic rays. It is also believed that AGN could be sites of ultra-high-energy (UHE) neutrino production. These would be produced in the interactions of UHE charged particles among themselves and with the ambient photons. Therefore, under the assumption that cosmic-ray emission is accompanied by neutrino emission, Auger's claim can be used to normalise the neutrino flux predicted by astrophysical models of AGN.

In the present work, we have focused on two such models of neutrino production that take into account Auger's results: one by H. B. J. Koers & P. Tinyakov [11] and another one by J. Becker & P. L. Biermann [12], which we will call hereafter the KT and BB models, respectively. They differ greatly in their assumptions and, within some regions of their parameter spaces, on their predictions of the neutrino fluxes. We have assessed the possibility of observing these two fluxes at the km-scale IceCube neutrino telescope in the South Pole, by allowing their respective model parameters to vary within given boundaries, and calculating the corresponding number of high-energy muon-neutrinos expected at the detector. In doing this, we have taken into account the present experimental upper bound on the neutrino flux set by AMANDA, and predicted bounds that IceCube, in its 40- and 80-strings configurations, would set in the event of non-observation of high-energy astrophysical neutrinos. Furthermore, we have also explored the parameter space for regions where the event-number predictions from the two production models can be distinguished from each other.

The remaining of the paper is divided as follows. In Section II, we describe the salient features of the KT and BB models, and show explicitly how the observations from the PAO enter the flux normalisation. Section III introduces current and envisioned experimental bounds on the high-energy extra-terrestrial neutrino flux. In Section IV we allow the parameters in the KT and BB models to vary within given bounds, and calculate the number of muon-neutrinos at IceCube predicted by each, while, in Section V, we present comparative plots of the two models in parameter space. We summarise and conclude in Section VI.

II. TWO MODELS OF NEUTRINO PRODUCTION AT AGN

High-energy gamma ray experiments such as HESS [13–15], MAGIC [16–19], VERITAS [20–22], and Milagro [23, 24] have observed during the last decade events with energies ranging from ~ 100 GeV to several TeV coming from identified extragalactic sources, notably AGN and Gamma Ray Bursts. While the correlation between observed gamma rays and catalogue sources is strong (signals at separation of 5σ or more from the background are not unusual), the generating mechanism of these emissions remains unknown [25]: high-energy gamma rays may be created at the sources as synchrotron radiation, in inverse Compton processes or in the decay of neutral pions resulting from pp and $p\gamma$ collisions. Current data are not sufficient to distinguish between these scenarios. The observation of neutrino emission correlated with the gamma-ray emission from these sources, however, would be enough to establish the decay of pions generated in the interactions of high-energy protons (and nuclei) as the generating mechanism: the same processes that create the neutral pions are also expected to create charged pions which would decay into neutrinos, yielding both a gamma-ray and a neutrino signal from the source, with the neutrino energy about a factor of two or three below the gamma-ray energy. Neutrino telescopes such as AMANDA [26], IceCube [27] and ANTARES [28] have been designed to detect this high-energy neutrino emission and, if possible, to correlate it with the known positions of gamma-ray sources.

AGN have long been presumed to be sites of high-energy neutrino production. In the scenario of neutrino production by meson decay, it is assumed that within the AGN protons are accelerated through first-order Fermi shock acceleration [6] and that pions are produced in the processes

$$p + \gamma \rightarrow \Delta^+ \rightarrow \begin{cases} p + \pi^0 \\ n + \pi^+ \end{cases} \quad , \quad n + \gamma \rightarrow p + \pi^- \quad , \quad (1)$$

with branching ratios $\text{Br}(\Delta^+ \rightarrow p\pi^0) = 2/3$ and $\text{Br}(\Delta^+ \rightarrow n\pi^+) = 1/3$. The neutral pions decay into gamma rays through $\pi^0 \rightarrow \gamma\gamma$, while the charged pions decay into electron and muon neutrinos through

$$\pi^+ \rightarrow \nu_\mu + \mu^+ \rightarrow e^+ + \nu_e + \bar{\nu}_\mu \quad , \quad \pi^- \rightarrow \bar{\nu}_\mu + \mu^- \rightarrow e^- + \bar{\nu}_e + \nu_\mu \quad . \quad (2)$$

The gamma rays thus created may be obscured and dispersed by the medium, and the protons will in addition be deviated by extragalactic magnetic fields on their journey to Earth. Neutrinos, on the other hand, escape from the production site virtually unaffected by interactions with the medium, so that, if their direction can be reconstructed at detection, they could point back to their sources.

If neutrinos are produced by charged pion decay, then, from Eq. (2), the ratios of the different flavours ($\nu_x + \bar{\nu}_x$) to the total flux are

$$\phi_{\nu_e}^0 : \phi_{\nu_\mu}^0 : \phi_{\nu_\tau}^0 = 1 : 2 : 0 . \quad (3)$$

Note, however, that these ratios are approximate; a detailed analysis of the pion decay and the contribution from higher-energy processes, such as the one in [29], will nevertheless result in values that are close to these standard ratios. Furthermore, ν_τ can be produced by the decay of D_s^\pm charmed mesons that are generated also in pp and $p\gamma$ collisions. The production of D_s^\pm is strongly suppressed, though, with $\phi_{\nu_\tau}^0 \approx 10^{-5}$ [30]. By the time neutrinos reach Earth, standard mass-driven neutrino oscillations will have distributed the total flux equally among the three flavours so that, at detection,

$$\phi_{\nu_e} : \phi_{\nu_\mu} : \phi_{\nu_\tau} = 1 : 1 : 1 . \quad (4)$$

New physics effects, such as neutrino decay [31], decoherence [32], or violation of Lorentz invariance or of CPT [33–35], could in principle result in large deviations from these ratios. In the present work, we have assumed that the ratios at production and detection are given, respectively, by their standard values, Eqs. (3) and (4).

In what follows, we will present in detail two representative models of UHE neutrino production at AGN, one by Koers & Tinyakov and the other by Becker & Biermann, both of which make use of the apparent correlation between the directions of UHECRs and the positions of known AGN reported by the PAO in order to calculate the normalisation of the diffuse neutrino flux.

A. Cosmic ray flux normalisation using results from Auger

The preferred mechanism for cosmic-ray acceleration at AGN is first-order Fermi acceleration [6], which results in a power-law differential cosmic ray proton spectrum,

$$\phi_p(E) \equiv \frac{dN_p}{dE} = A_p E^{-\alpha_p} , \quad (5)$$

with E the cosmic-ray energy at detection on Earth. Here, A_p is the energy-independent normalisation constant. The integral of this expression,

$$N(E_{\text{th}}) = \int_{E_{\text{th}}} \frac{dN_p}{dE} dE \simeq A_p (\alpha_p - 1)^{-1} E_{\text{th}}^{\alpha_p - 1} , \quad (6)$$

is the integrated cosmic ray flux above a certain threshold energy E_{th} . For the UHECRs detected at Auger, $E_{\text{th}} = 57$ EeV.

On the other hand, the integrated flux can be calculated from experimental data as

$$N(E_{\text{th}}) = N_{\text{evts}}(E_{\text{th}}) / \Xi . \quad (7)$$

where $N_{\text{evts}}(E_{\text{th}})$ is the number of observed cosmic rays above E_{th} and $\Xi = 9000 \text{ km}^2 \text{ yr sr}$ is the reported [7] total detector exposure of Auger. The KT and BB models use different values for $N_{\text{evts}}(E_{\text{th}})$, according to their assumptions: KT assumes $N_{\text{evts}} = 2$ originated at Cen A and uses this to calculate the diffuse neutrino flux assuming that all AGN behave like Cen A, while BB assumes that the $N_{\text{evts}} = 20$ events truly originated at the AGN with which the correlation was found. Combining this expression with Eq. (6) yields for the normalisation constant,

$$A_p = \frac{N_{\text{evts}}(\alpha_p - 1)}{\Xi} E_{\text{th}}^{\alpha_p - 1} . \quad (8)$$

The spectral index α_p is expected to lie between 2 and 3 and is treated in the present work as a free parameter with values in this range. We will see in the next two subsections that the relation between the cosmic-ray normalisation constant and the neutrino normalisation constant is model-dependent.

When calculating the proton spectrum from a single point source, we will need to weigh the normalisation constant using the detector effective area A that is accessible to the observation, which depends on the declination δ_s of the source, i.e.,

$$A_p^{\text{pt}} = \frac{N_{\text{evts}}(\alpha_p - 1)}{\Xi} E_{\text{th}}^{\alpha_p - 1} \frac{\int A(\delta_s) d\Omega}{A(\delta_s)} . \quad (9)$$

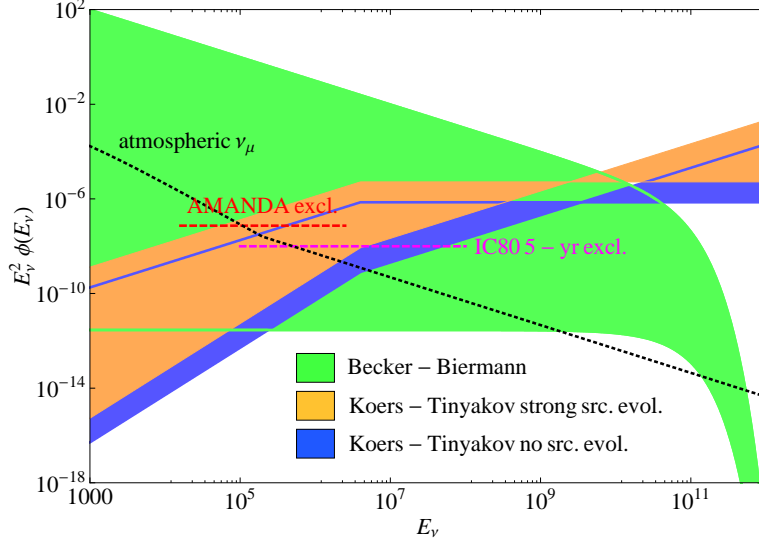


FIG. 1: AGN ν_μ fluxes, multiplied by E_ν^2 , according to the models by Becker & Biermann (BB) and Koers & Tinyakov (KT), with strong source evolution and without source evolution. The regions were generated by varying the model parameters in the ranges $2 \leq \alpha \leq 3$, $1 \leq \Gamma_\nu/\Gamma_{\text{CR}} \leq 20$, and $10^{-3} \leq z_{\text{CR}}^{\text{max}} \leq 0.03$. The green region corresponds to all the possible BB fluxes resulting from the variation of α , $\Gamma_\nu/\Gamma_{\text{CR}}$, and $z_{\text{CR}}^{\text{max}}$, whereas the blue and orange regions correspond to all the possible KT fluxes resulting from the variation of α , under the assumption of no source evolution and of strong source evolution, respectively. The atmospheric muon-neutrino flux has been plotted (in black, dotted, lines) for comparison. The existing AMANDA upper bound and the projected full-IceCube (IC80) five-years bounds have been plotted by assuming a E_ν^{-2} flux. See the text for details.

B. Model by Koers & Tinyakov

The PAO has reported [7] observing two UHECR events correlated with the position of Centaurus A (Cen A), the nearest active galaxy, lying at about 3.5 Mpc. The observed differential flux from a point source lying at proper (luminosity) distance $d_L(z)$ is

$$\phi(E) = \frac{j^0(E_0)}{4\pi d_L^2(1+z)} \frac{dE_0}{dE}, \quad (10)$$

where E is the observed energy and the energy at the source, $E_0 = E_0(E, z)$, is calculated taking into account energy losses. We denote by j^0 the differential injected spectrum at the source, which for protons and neutrinos behaves like a power-law, i.e., $j_p^0 \propto E^{-\alpha_p}$, $j_\nu^0 \propto E^{-\alpha_\nu}$, respectively. The KT model [7] assumes that Cen A is a typical source of UHECRs and neutrinos, and computes the diffuse flux under the assumption that all sources are identical to Cen A by integrating over a cosmological distribution of sources, while taking into account energy losses during the propagation of the particles. Thus, the diffuse flux of a particle species is

$$\phi^{\text{diff}}(E) = \frac{cn_0}{4\pi} \int_0^\infty dz \left| \frac{dt}{dz} \right| \frac{dE_0}{dE} \epsilon(z) j^0(E_0), \quad (11)$$

where c is the speed of light, n_0 is the local source density and $\epsilon(z)$ parametrises the source distribution. Two limiting cases have been considered: one in which there is no source evolution with redshift ($\epsilon(z) = 1$) and another one, adopted from [36], in which there is a strong source evolution which follows the star formation rate,

$$\epsilon(z) \propto \begin{cases} (1+z)^{3.4} & , \text{ if } z \leq 1.9 \\ (1+1.9)^{3.4} & , \text{ if } 1.9 < z < 3 \\ (z-3)^{-0.33} & , \text{ if } z \geq 3 \end{cases}. \quad (12)$$

The KT model adopts the Λ CDM cosmology to calculate $|dt/dz|^{-1} = H_0(1+z) \sqrt{\Omega_m(1+z)^3 + \Omega_\Lambda}$, with $H_0 = 73 \text{ km s}^{-1} \text{ Mpc}^{-1}$ the Hubble constant and $\Omega_m = 0.24$, $\Omega_\Lambda = 0.76$ the present matter density and vacuum energy density parameters, respectively.

The diffuse neutrino flux is normalised using the integrated UHECR flux $\Phi_p^{\text{diff}}(E_{\text{th}})$ above the threshold E_{th} ,

$$\frac{\phi_\nu^{\text{diff}}(E_\nu)}{j_\nu^0(E_\nu)} = H(E_{\text{th}}) \frac{\Phi_p^{\text{diff}}(E_{\text{th}})}{J_p^0(E_{\text{th}})}, \quad (13)$$

with $J_p^0(E_{\text{th}})$ the integrated UHECR proton spectrum at the source. The proportionality constant, $H(E_{\text{th}})$, is called the “neutrino boost factor” and contains the information on neutrino mean free path lengths and source evolution. It can be calculated numerically, provided an expression is given for dE_0/dE , from Eqs. (11) and (13). Proton energy losses are taken into account in the continuous-loss approximation, considering both loss by the adiabatic expansion of the Universe and loss from interactions with the CMB photons resulting in pion photoproduction and electron-positron pair production; see Appendix A in Ref. [11] for details. To obtain the diffuse flux, the source distribution is integrated up to $z = 5$.

The PAO energy threshold is $E_{\text{th}} = 57$ EeV. However there is a $\sim 20\%$ systematic uncertainty in the energy determination that affects the neutrino boost factor. Koers & Tinyakov [11] found that this uncertainty is well approximated by

$$H'(E_{\text{th}}) = 10^{(E_{\text{th}}/E_0)-1} H(E_0), \quad (14)$$

where E_{th} is the actual threshold and $E_0 = 57$ EeV. This introduces a variation in H of a factor of ~ 1.6 when the energy is mis-reconstructed with 20% accuracy.

The integrated diffuse UHECR neutrino spectrum and the integrated flux from Cen A above 57 EeV can be written, respectively, as

$$\Phi_p^{\text{diff}}(E_{\text{th}}) = \frac{N_{\text{tot}} - N_{\text{Cen A}}}{\Xi} = 9 \times 10^{-21} \text{ cm}^{-2} \text{ s}^{-1} \text{ sr}^{-1} \quad (15)$$

$$\Phi_p^{\text{Cen A}}(E_{\text{th}}) = \frac{N_{\text{Cen A}}}{\Xi} \frac{\int A(\delta_s) d\Omega}{A(\delta_s)} = 5 \times 10^{-21} \text{ cm}^{-2} \text{ s}^{-1} \text{ sr}^{-1}, \quad (16)$$

where $\delta_s = -43^\circ$ is the declination of Cen A and $A(\delta_s)$ is the detector’s effective area for this declination. The PAO reported $A(\delta_s) / \int A(\delta_s) d\Omega = 0.15 \text{ sr}^{-1}$ and $N_{\text{tot}} = 27$ events above 57 EeV, with $N_{\text{Cen A}} = 2$ of these coming from the direction of Cen A. From Eq. (13), we find

$$\frac{\phi_\nu^{\text{diff}}(E_\nu)}{\phi_p^{\text{Cen A}}(E_\nu)} = H'(E_{\text{th}}) \frac{\Phi_p^{\text{diff}}(E_{\text{th}})}{\Phi_p^{\text{Cen A}}(E_{\text{th}})} = H'(E_{\text{th}}) \frac{N_{\text{tot}} - N_{\text{Cen A}}}{N_{\text{Cen A}}} \frac{A(\delta_s)}{\int A(\delta_s) d\Omega} \simeq 1.9 H'(E_{\text{th}}). \quad (17)$$

This relation between the diffuse neutrino flux and the flux from Cen A is the main result of the KT model.

In their paper [11], Koers & Tinyakov used a model by Cuoco & Hannestad [37] to describe the neutrino emission from Cen A, $\phi_\nu^{\text{Cen A}}$, itself based on a model by Mannheim, Protheroe & Raschen [38]. In this model, it is assumed that high-energy protons, accelerated by some mechanism (e.g., shock acceleration) are confined within a region close to the source. Because of energy losses in their photopion interactions with the ambient photon field, which is assumed to have an energy spectrum $n(\epsilon_\gamma) \propto \epsilon_\gamma^{-2}$, their lifetime is much shorter than their diffusive escape time and they decay into neutrons and neutrinos, both of which escape the source. Thereafter, the neutrons decay into UHECR protons; however, because of their interaction with the photon field before decaying, the neutrons produce a softer proton spectrum than the seed proton spectrum. Furthermore, the model predicts two spectral breaks in the CR spectrum, at energies at which the optical depths for proton and neutrino photopion production become unity. These two breaks are close in energy, though, so that to simplify the model, only one spectral break is considered, at energy E_{br} . Below E_{br} , the UHECR proton and neutrino spectra are harder than the seed proton spectra by one power of the energy, while above E_{br} , the UHECR proton spectrum is softer than the seed proton by one power of the energy and the neutrino spectrum is harder by one power of the energy. Hence, at high energies, the model predicts a neutrino spectrum that is harder by one power of the energy than the UHECR proton spectrum.

Following [11, 37, 38], the all-flavour neutrino spectrum from Cen A can be written as

$$\phi_\nu^{\text{Cen A}}(E_\nu) = \frac{\xi_\nu}{\xi_n \eta_{\nu n}^2} \min\left(\frac{E_\nu}{\eta_{\nu n} E_{\text{br}}}, \frac{E_\nu^2}{\eta_{\nu n}^2 E_{\text{br}}^2}\right) \phi_p^{\text{Cen A}}\left(\frac{E_\nu}{\eta_{\nu n}}\right), \quad (18)$$

where ξ_i ($i = \nu, n$) is the fraction of the proton’s energy that is transferred to the species i in photopion interactions and $\eta_{\nu n}$ is the ratio of the average neutrino energy to the average neutron energy. The KT model uses for these parameters the values featured in [38], obtained from Monte Carlo simulations: $\xi_\nu \approx 0.1$, $\xi_n \approx 0.5$, $\langle E_\nu \rangle / E_p \approx 0.033$ and $\langle E_n \rangle / E_p \approx 0.83$, with which

$$\xi_\nu / \xi_n = 0.2 \quad , \quad \eta_{\nu n} = 0.04. \quad (19)$$

The neutrino break energy, E_{br} , is estimated from the gamma-ray break energy as $E_{\text{br}} \simeq 3 \times 10^8 E_{\gamma, \text{br}}$. Ref. [38] uses $E_{\gamma, \text{br}} = 200$ MeV, so that

$$E_{\text{br}} = 10^8 \text{ GeV} . \quad (20)$$

Under the assumption of equitative flavour ratios at Earth (see Section I), the $\nu_\mu + \bar{\nu}_\mu$ flux is 1/3 the flux in Eq. (18). Plugging the power-law proton spectrum, Eq. (5), with the normalisation constant for a point source, Eq. (9), yields

$$\phi_{\nu_\mu}^{\text{Cen A}}(E_\nu) = \frac{\Phi_p^{\text{Cen A}}(E_{\text{th}})}{3} \frac{\xi_\nu \eta_{\nu n}^{\alpha_p - 2}}{\xi_n} \frac{\alpha_p - 1}{E_{\text{th}}} \left(\frac{E_\nu}{E_{\text{th}}} \right)^{-\alpha_p} \left(\frac{E_\nu}{E_{\nu, \text{br}}} \right) \min \left(1, \frac{E_\nu}{E_{\nu, \text{br}}} \right) \quad (21)$$

for the muon-neutrino flux from Cen A, with $E_{\nu, \text{br}} \equiv \eta_{\nu n} E_{\text{br}} = 4 \times 10^6$ GeV. While Koers & Tinyakov [11] considered mainly a proton spectral index $\alpha_p = 2.7$, we have considered α_p a free parameter of the model and, as we will see in Sections IV and V, we have allowed it to vary in the interval $2 \leq \alpha_p \leq 3$. Giving values to the rest of the parameters, the muon-neutrino flux from Cen A results in

$$\phi_{\nu_\mu}^{\text{Cen A}}(E_\nu) \simeq 9.14 \times 10^{-37} \times (2.28 \times 10^9)^{\alpha_p} (\alpha_p - 1) E_\nu^{1-\alpha_p} \min \left(1, \frac{E_\nu}{E_{\nu, \text{br}}} \right) . \quad (22)$$

Using the scaling relation, Eq. (17), the muon-neutrino diffuse flux in the KT model is therefore

$$\phi_{\nu_\mu}^{\text{diff, KT}}(E_\nu) \simeq 1.9 H'(E_{\text{th}}) \phi_{\nu_\mu}^{\text{Cen A}}(E_\nu) . \quad (23)$$

The variation of H' with α_p , for both assumptions on source evolution, is shown in Figure 1 of Ref. [11].

C. Model by Becker & Biermann

The BB model [12] describes the production of high-energy neutrinos in the relativistic jets of radio galaxies. According to the model, the UHECRs observed by the PAO originated at FR-I galaxies (relatively low-luminosity radio galaxies with extended radio jets, and radio knots distributed along them), which can in principle accelerate protons up to $\sim 10^{20}$ eV. Like in the KT model, here the protons are also shock-accelerated. Unlike the KT model, though, where the neutrino emission occurred in a region close to the AGN core, in the BB model the neutrino emission from $p\gamma$ interactions is expected to peak at the first strong shock along the jet, lying at a distance of $z_j \sim 3000$ gravitational radii from the center.

The optical depth corresponding to proton interactions with the disc photon field, $\tau_{p\gamma_{\text{disc}}} \equiv 1/\lambda_{p\gamma_{\text{disc}}} = z_j \theta n_{\gamma_{\text{disc}}} \sigma_{p\gamma}$, for a source with disc luminosity $L_{\text{disc}} \sim 10^{44}$ erg s $^{-1}$, is [12]

$$\tau_{p\gamma_{\text{disc}}} = 0.2 \epsilon_{\text{Edd}} \left(\frac{\theta}{0.1} \right) \left(\frac{z_j}{3000 r_g} \right)^{-1} \left(\frac{L_{\text{disc}}}{10^{44} \text{ erg s}^{-1}} \right) , \quad (24)$$

where $\sigma_{p\gamma} \approx 900 \mu\text{barn}$ is the total $p\gamma$ cross-section for the production of the Δ^+ resonance, $\epsilon_{\text{Edd}} \leq 1$ is the accretion rate relative to the maximum, θ is the beam aperture angle, and the gravitational radius $r_g = 1.5 \times 10^{12} M_{\text{BH}} / (10^7 M_\odot)$ cm, with M_{BH} and M_\odot the mass of the central supermassive black hole and of the Sun, respectively. The photon density is calculated as

$$n_{\gamma_{\text{disc}}} = \frac{L_{\text{disc}}}{4\pi z_j^2 c h \nu} , \quad (25)$$

where h is Planck's constant and the average photon energy in the disc $h\nu = 20$ eV. For $\epsilon_{\text{Edd}} = 0.1$, the optical depth is $\tau_{p\gamma_{\text{disc}}} \approx 0.02$, and so $p\gamma$ interactions in the disc are not the dominant source of neutrinos. The proton-proton interactions that occur when the jet encounters the AGN's torus, at $z_j \sim 1 - 10$ pc, are also subdominant: given the torus column density $X \sim 4 \times 10^{23} \text{ cm}^{-2}$ and the pp cross section $\sigma_{pp} \approx 50$ mb, the optical depth results

$$\tau_{pp_{\text{torus}}} = X \sigma_{pp} \approx 2 \times 10^{-3} . \quad (26)$$

Thus, pp interactions are neglected in the BB model.

The dominant mechanism of neutrino production is the interaction between the accelerated protons and the synchrotron photons in the relativistic jet, at one of the jet's knots, which is assumed to contribute a fraction $\epsilon_{\text{knot}} \approx 0.1$ of the total synchrotron luminosity, $L_{\text{synch}} \sim 10^{40}$ erg s $^{-1}$. In this case, the optical depth is given by [12]

$$\tau_{p\gamma_{\text{synch}}} \approx 0.9 \left(\frac{10}{\Gamma} \right) \left(\frac{\theta}{0.1} \right) \left(\frac{\epsilon_{\text{knot}}}{0.1} \right) \left(\frac{L_{\text{synch}}}{10^{40} \text{ erg s}^{-1}} \right) \left(\frac{z_j}{3000 r_g} \right)^{-1} \left(\frac{\nu}{1 \text{ GHz}} \right)^{-1} , \quad (27)$$

where $\nu \approx 1$ GHz is the frequency of the synchrotron photons. For boost factors of $\Gamma \sim 10$, the optical depth $\tau_{p\gamma_{\text{synch}}} \sim 1$. Hence, it is expected that neutrino emission occurs predominantly at the foot of the jet, where the beam is still highly collimated. Therefore, the BB model predicts a highly beamed neutrino emission, produced in the first shock ($z_j \sim 3000r_g$), and consequently observable only from sources whose jets are directed towards Earth. Flat-spectrum radio sources, such as FR-I galaxies whose jets are pointing towards Earth, will have correlated neutrino and proton spectra, while steep-spectrum sources, which are AGN seen from the side, are expected to be weak neutrino sources, but to contribute to the cosmic-ray proton flux.

The BB model assumes that the $N_{\text{evts}} = 20$ events that were observed by the PAO to have a positional correlation to sources in the Véron-Cetty & Véron catalogue were indeed originated at AGN lying in the supergalactic plane. The normalisation constant of the proton spectrum, A_p , is given by Eq. (8) with this value for N_{evts} . We now need a connection between A_p and the corresponding normalisation constant for neutrinos, A_ν . To this end, consider the total neutrino and total proton energy fluxes radiated in the solid angles Ω_ν and Ω_p , respectively, in the shock rest frame (i.e., denoted by primed variables):

$$\Omega_\nu j'_\nu = \int E'_\nu \frac{dN_\nu}{dE'_\nu} dE'_\nu \quad , \quad \Omega_p j'_p = \int E'_p \frac{dN_p}{dE'_p} dE'_p \quad . \quad (28)$$

These are connected by

$$\Omega_\nu j'_\nu = \frac{\tau_{p\gamma}}{12} \Omega_p j'_p \quad , \quad (29)$$

where the factor $1/12$ is due to the branching ratio of Δ^+ to charged pions ($1/3$, see Eq. (1)), to the fact that half of the energy of the pion is transferred to the muon neutrinos ($\nu_\mu + \bar{\nu}_\mu$), and to the oscillation of half of the muon-flavoured neutrinos into the other two flavours. The energy fluxes at Earth are given by

$$j = \frac{\Gamma}{4\pi} j' n \quad , \quad (30)$$

where

$$j' \equiv \int_{E'} dE' E' \frac{dN}{dE'} \quad (31)$$

is the energy flux in the shock rest frame and

$$n \equiv \int_{z_{\text{min}}}^{z_{\text{max}}} \int_{L_{\text{min}}}^{L_{\text{max}}} dz dL \frac{1}{4\pi d_L^2(z)} \frac{d^2 n}{dV dL} \frac{dV}{dz} \quad (32)$$

is the total number of sources. In this last expression, d_L is the luminosity distance of the source, $d^2 n/dV dL$ is the luminosity function of the sources (the distribution of sources as a function of redshift and luminosity), and dV/dL is the differential comoving volume. Because strong neutrino sources are weak CR proton sources, the luminosity function will be different for neutrinos and protons: for the former, the model assumes the FR-I radio luminosity function by Willot [39], while for the latter, the luminosity function by Dunlop & Peacock is employed [40]. The lower redshift integration limit for CR proton sources, $z_{\text{CR}}^{\text{min}} = 0.0008$, corresponds to the closest FR-I source, Cen A, while the one for neutrinos, $z_\nu^{\text{min}} = 0.018$, corresponds to the closest FRS source, Perseus A. The absolute upper integration limit, $z_{\text{CR}}^{\text{max}} = 0.03$, marks the outskirts of the supergalactic plane and is thus common for both neutrinos and protons; we will, however, maintain $z_{\text{CR}}^{\text{max}}$ as a free parameter in our analysis, with 0.03 as its maximum value. The luminosity integration limits, $L_{\text{min}} = 10^{40} \text{ erg s}^{-1}$ and $L_{\text{max}} = 10^{44} \text{ erg s}^{-1}$, are obtained from the distribution of FR-I galaxies (FRS galaxies are believed to be a subclass of FR-I, so the limits apply to them as well [12]). Replacing the expressions for the energy fluxes in Eq. (29) yields

$$j_\nu = \frac{\tau_{p\gamma}}{12} \frac{\Gamma_\nu}{\Gamma_{\text{CR}}} \frac{\Omega_p}{\Omega_\nu} \frac{n_\nu}{n_p} (z_{\text{CR}}^{\text{max}}) j_p \quad . \quad (33)$$

The dependence of n_ν/n_p on $z_{\text{CR}}^{\text{max}}$ is shown graphically in Figure 5 of [12]. In addition to $z_{\text{CR}}^{\text{max}}$, we have maintained the ratio of boost factors, $\Gamma_\nu/\Gamma_{\text{CR}}$, as a free parameter of the BB model.

On the other hand, assuming a power-law behaviour for the diffuse differential flux of protons, i.e., $\phi_p^{\text{diff}} \equiv dN_p/dE_p = A_p E_p^{-\alpha_p}$, the integrated energy flux results

$$j_p = A_p \int_{E_{p,\text{min}}}^{E_{p,\text{max}}} E_p \frac{dN_p}{dE_p} dE_p = \begin{cases} A_p (\alpha_p - 2)^{-1} E_{p,\text{min}}^{-\alpha_p+2} & , \text{ if } \alpha_p \neq 2 \\ A_p \ln(E_{p,\text{max}}/E_{p,\text{min}}) & , \text{ if } \alpha_p = 2 \end{cases} \quad , \quad (34)$$

where the term proportional to $E_{p,\max}^{-\alpha_p+2}$ has been neglected, in the case when $\alpha_p \neq 2$. The normalisation constant A_p is given by Eq. (8). Assuming that the neutrino spectrum follows the proton spectrum, i.e., $\phi_{\nu\mu}^{\text{diff,BB}} = A_\nu E_\nu^{-\alpha_\nu}$ with $\alpha_\nu \approx \alpha_p$, the energy flux for neutrinos is

$$j_\nu \simeq \begin{cases} A_\nu (\alpha_p - 2)^{-1} E_{\nu,\min}^{-\alpha_p+2} & , \text{ if } \alpha_p \neq 2 \\ A_\nu \ln(E_{\nu,\max}/E_{\nu,\min}) & , \text{ if } \alpha_p = 2 \end{cases} . \quad (35)$$

The lower integration limits for protons and neutrinos are, respectively, $E_{p,\min} = \Gamma_p m_p \approx \Gamma_p \cdot (1 \text{ GeV})$ and $E_{\nu,\min} = \Gamma_\nu \cdot (m_\pi/4) = \Gamma_\nu \cdot (0.035 \text{ GeV})$. Finally, we see that when $\alpha_p \neq 2$, the neutrino normalisation constant is given by

$$A_\nu \simeq \frac{\tau_{p\gamma}}{12} \left(\frac{\Gamma_\nu}{\Gamma_p} \right)^{\alpha_p+1} \frac{n_\nu}{n_p} (z_{\text{CR}}^{\max}) \left(\frac{m_\pi}{4} \right)^{\alpha_p-2} \frac{N_{\text{evts}}(\alpha_p - 1)}{\Xi} E_{\text{th}}^{\alpha_p-1} . \quad (36)$$

To arrive at this expression¹, it must be noted that because of the relativistic beaming in the jets, the emission solid angles are $\Omega_\nu \sim 1/\Gamma_\nu^2$ and $\Omega_p \sim 1/\Gamma_{\text{CR}}^2$. When $\alpha_p = 2$, the logarithms in the two spectra are similar and cancel out, making the previous expression for A_ν valid also for $\alpha_p = 2$.

Figure 1 shows the BB and KT fluxes, multiplied by E_ν^2 , as functions of the neutrino energy, when the values of the model parameters are varied within the ranges that we have used in our analysis (see Section IV): $2 \leq \alpha \leq 3$, $1 \leq \Gamma_\nu/\Gamma_{\text{CR}} \leq 20$, and $10^{-3} \leq z_{\text{CR}}^{\max} \leq 0.03$ (to simplify, we will use $\alpha \equiv \alpha_p$ hereafter). We have also included the current upper bound on the flux, set by the AMANDA Collaboration [42], and the projected sensitivity of the completed IceCube detector (IC80) after five years of running [43]. We will introduce these bounds in detail in Section III. For now, suffice it to say that our analysis, in Sections IV and V, will focus on the region between the IC80 lower bound and the AMANDA upper bound, in the energy range 10^5 – 10^8 GeV, where the fluxes may be detected at IceCube. We will find how the bounds on the neutrino flux translate into bounds on the values of α , $\Gamma_\nu/\Gamma_{\text{CR}}$, and z_{CR}^{\max} , thus restricting the capacity of the KT and BB flux models to account for an observed extra-terrestrial neutrino signal.

III. CURRENT AND ENVISIONED BOUNDS ON THE NEUTRINO FLUX

In the present work, we have assumed that the UHE AGN neutrino flux accounts for all of the UHE neutrino flux. This is, of course, a simplifying assumption, since high-energy contributions could also originate at other types of sources, such as supernova remnants [44].

A. Current bound from AMANDA and projected IceCube-80 bounds

Currently, the most stringent upper bound on the diffuse high-energy flux of extra-terrestrial muon-neutrinos, between the energies 16 TeV – 2.5 PeV, is the one obtained by AMANDA from the analysis of data recorded between the years 2000 and 2004 [42]:

$$\text{AMANDA exclusion (reported): } \frac{1}{2.5 \text{ PeV} - 16 \text{ TeV}} \int_{16 \text{ TeV}}^{2.5 \text{ PeV}} E_\nu^2 \phi_{\nu\mu}^{\text{diff}}(E_\nu) = 7.4 \times 10^{-8} \text{ GeV cm}^{-2} \text{ s}^{-1} \text{ sr}^{-1} . \quad (37)$$

Since the relatively small effective detector area of AMANDA was insufficient to separate downgoing neutrinos from the atmospheric muon background, this bound was set using exclusively upgoing UHE neutrinos, six of which were detected during the 807 days of live time reported.

The expected sensitivity to the extra-terrestrial muon-neutrino flux that the full, 80-string, IceCube detector is expected to achieve after five years of exposure, i.e., the minimum necessary flux for a 5σ discovery, is [43]

$$\text{IC80 5-yr discovery (projected): } \frac{1}{10^8 - 10^5 \text{ GeV}} \int_{10^5 \text{ GeV}}^{10^8 \text{ GeV}} E_\nu^2 \phi_{\nu\mu}^{\text{diff}}(E_\nu) = 9.9 \times 10^{-9} \text{ GeV cm}^{-2} \text{ s}^{-1} \text{ sr}^{-1} . \quad (38)$$

We will use this sensitivity as a lower bound on the neutrino flux.

¹ The reader should be wary that in their paper [12], Becker & Biermann incorrectly reported a dependence of the form $\sim (\Gamma_\nu/\Gamma_{\text{CR}})^{5-\alpha_p}$ [41].

Limit	Energy range [GeV]	Exposure time	Upgoing	Downgoing
AMANDA exclusion reported (AMANDA) [42]	$1.6 \times 10^4 - 2.5 \times 10^6$	807 days	6.0	–
IC40 exclusion estimated (IC40NS)	$10^{4.5} - 10^7$	1 yr	53.58	30.35
IC80 sensitivity projected (IC80PS) [43]	$10^5 - 10^8$	5 yr	113.61	41.46

TABLE I: Maximum number of upgoing and downgoing muon-neutrinos allowed by the reported exclusion limit from AMANDA and by our estimated exclusion limit assuming no signal observation after one year of running IC40, and minimum number of events needed for 5σ discovery according to the projected IC80 5-year analysis. Each upper bound on the number of events is calculated in the respective detector configuration (Appendix A contains the effective area for each), with the corresponding exposure time. The event numbers associated to the IC80 sensitivity were calculated by assuming a E_ν^{-2} diffuse flux.

We wish to find the minimum allowed number of ν_μ at IC80, after five years of exposure, that will be necessary for a 5σ signal discovery, according to Eq. (38). In order to do this, we have assumed a $\phi_{\nu_\mu}^{\text{diff}}(E_\nu) = kE_\nu^{-2}$ flux, with the normalisation, k , given by the numerical value of the integral in Eq. (38), in units of $\text{GeV}^{-1} \text{cm}^{-2} \text{s}^{-1} \text{sr}^{-1}$. The expressions required to calculate the number of upgoing and downgoing muon-neutrinos at the full IC80 array, for an arbitrary diffuse neutrino flux $\phi_{\nu_\mu}^{\text{diff}}$, are contained in Appendix A. We have thus calculated the minimum number of events, for downgoing and upgoing neutrinos, associated to the IC80PS sensitivity, and presented the results in Table I. For the AMANDA exclusion, the six events reported can be reproduced using the expressions in Appendix A valid for upgoing neutrinos, with a E_ν^{-2} flux, and with the effective area a factor of 100 lower than the IC80 effective area.

B. An estimated upper bound from IceCube-40

The complete IceCube array is expected to be finished in the 2010-2011 season. In the meantime, the 40-string configuration of IceCube (IC40) ran for little more than a year, collecting data the analysis of which has not yet been reported. By assuming that IC40 did not observe a statistically significant signal corresponding to a high-energy extra-terrestrial neutrino flux, we are able to estimate an upper bound on the number of muon-neutrinos to be expected at the full IceCube array, which will be more stringent than the AMANDA bound. In Ref. [45], the preliminary IC40 sensitivity was estimated within the energy range $10^{4.7} \leq E_\nu/\text{GeV} \leq 10^7$; we have chosen the same range for our estimated IC40 upper bound. In order to find the upper bound, we have set the exposure time to 1 year and defined the signal-to-noise ratio as the ratio of the number of extra-terrestrial muon-neutrinos with energies within $10^{4.5} - 10^7$ GeV, $N_{\text{1yr}}^{\text{IC40}}$, to the square root of the number of atmospheric muon-neutrinos, $N_{\text{atm,1yr}}^{\text{IC40}}$, i.e.,

$$r = N_{\text{1yr}}^{\text{IC40}} / \sqrt{N_{\text{atm,1yr}}^{\text{IC40}}} , \quad (39)$$

and defined the upper bound on $N_{\text{1yr}}^{\text{IC40}}$ as its value at $r = 3$. Following [11], we parametrise the muon-neutrino atmospheric background (in units of $\text{GeV}^{-1} \text{cm}^{-2} \text{s}^{-1} \text{sr}^{-1}$) as

$$\Phi_\nu^{\text{atm}}(E_\nu) = \begin{cases} \frac{8.4 \times 10^{-2} (E_\nu/1 \text{ GeV})^{-2.74}}{1 + 2 \times 10^{-3} (E_\nu/1 \text{ GeV})} & , E_\nu < 10^{5.3} \text{ GeV} \\ 5.7 \times 10^{-3} (E_\nu/1 \text{ GeV})^{-3.01} & , E_\nu \geq 10^{5.3} \text{ GeV} \end{cases} , \quad (40)$$

with the higher-energy branch due to neutrino production by decay of charmed particles. Furthermore, we have assumed that the effective detector area in IC40 is half the area in IC80, the latter of which is the one used in Appendix A. At IC40, in one year of exposure, 319.02 (102.32) upgoing (downgoing) atmospheric events would be observed in the range $10^{4.7} - 10^7$ GeV. The IC40 upper bounds for upgoing and downgoing neutrinos are presented in the second line in Table I.

IV. MUON-NEUTRINO NUMBER OF EVENTS AT THE ICECUBE DETECTOR FOR THE BB AND KT MODELS

In this Section, we study the Koers & Tinyakov (KT) and the Becker & Biermann (BB) models of diffuse AGN neutrino flux through their predictions of the number of muon-neutrinos that will be detected at the full IceCube-80 neutrino detector. To calculate the number of ν_μ , we have adopted the method followed in [11], which is summarised here in Appendix A. In order to obtain our predictions, we have taken as free parameters α for the KT model, and

Limit	no source evolution		strong source evolution	
	upgoing	downgoing	upgoing	downgoing
AMANDA	3.04	(3.04)	2.80	(3.04)
IC40NS	2.88	2.91	2.59	2.61
IC80PS	2.64	2.54	2.29	2.13

TABLE II: Maximum value of the spectral index α in the Koers-Tinyakov model allowed by the exclusion limits from AMANDA and IC40 1-year, and minimum value needed for 5σ discovery according to the projected IC80 5-year analysis. Seeing as there was no downgoing sample examined at AMANDA, in our calculations we associate to it the same upper bound on α that as for the upgoing sample.

α , $\Gamma_\nu/\Gamma_{\text{CR}}$, and $z_{\text{CR}}^{\text{max}}$ for the BB model, and varied them within the following intervals:

$$2 \leq \alpha \leq 3, \quad 1 \leq \Gamma_\nu/\Gamma_{\text{CR}} \leq 20, \quad 10^{-3} \leq z_{\text{CR}}^{\text{max}} \leq 0.03. \quad (41)$$

This range of α has been chosen in order to cover a wide range around 2.7, the preferred value obtained from fits to combined cosmic-ray data [46]. The range of $\Gamma_\nu/\Gamma_{\text{CR}}$ is selected so that it includes the value of 3 quoted in [12], while the range of $z_{\text{CR}}^{\text{max}}$ is the same as the one used in said reference. Our purpose in varying the latter parameter, $z_{\text{CR}}^{\text{max}}$, is to probe different hypotheses about the maximum redshift up to which the AGN contribute to the UHE diffuse neutrino flux.

In our analysis, we have fixed the IC80 detector exposure time at $T = 5$ years and calculated the integrated event yield within the energy range $10^5 - 10^8$ GeV, while allowing for the two possible incoming directions: downgoing, where the neutrinos reach the detector with zenith angles between 0° and 90° (the normal to the South Pole lies at 0°) and upgoing, where the zenith angle lies between 90° and 180° . Downgoing neutrinos traverse only about 10 km of atmosphere before reaching the detector, while upgoing neutrinos traverse the whole or part of the Earth's diameter, and are influenced by matter effects. In the case of the KT flux, we have considered both the scenario with no source evolution and the one with strong source evolution.

Furthermore, we have explored two different visibility criteria which have the purpose of identifying the regions of parameter space allowed by the upper limits considered in this work and accessible by the sensitivity of the full IceCube array. In the first criterion –the AMANDA visibility criterion– the upper limit is fixed at the AMANDA bound, while, in the second criterion –the IC40 visibility criterion– it is fixed at our estimated IC40NS upper bound. For both criteria, the lower bound is given by the IC80PS sensitivity limit. The event-number sensitivity and upper bounds are contained in Table I. Since the KT flux depends on a single parameter, i.e., the spectral index α , we can translate the bounds on event numbers directly into bounds on α for the KT model. The results are presented in Table II.

A. KT event-rate expectations at IceCube-80

Figure 2 shows, under the assumption of a KT flux, the integrated number of muon-neutrinos with energies between 10^5 and 10^8 GeV, as a function of α , that is expected at the full 80-string IceCube array after five years of exposure. Plots (a) and (b) assume no source evolution, whereas (c) and (d) assume strong source evolution. Each plot contains both upgoing- and downgoing-neutrino event numbers. In all of these plots it is evident that for low values of α , the predictions for up- and downgoing neutrinos are close to each other, but they drift apart as α increases, with the number of upgoing events always higher than the number of downgoing events. Additionally, the event-number predictions under the assumption of strong source evolution are up to an order of magnitude higher than the predictions under no source evolution. This fact can be easily understood since a difference of a similar magnitude is found in the neutrino boost factor, as shown in [11].

In every plot, the yellow-coloured and hatched bands mark the visibility regions for downgoing and upgoing neutrinos, respectively. In plots (a) and (c), the bands are determined according to the IC40 visibility criterion, with the upper and lower limits given by the IC40NS and IC80PS bounds, respectively, for upgoing and downgoing neutrinos according to Table II. In plots (b) and (d), the bands are determined instead according to the AMANDA visibility criterion, with the upper limit fixed by the AMANDA upgoing sample, for both downgoing and upgoing neutrinos, and the lower limit given by the IC80PS sensitivity, which differs for upgoing and downgoing neutrinos according to Table II. Owing to the fact that the AMANDA upper bound is less restrictive than the IC40NS bound, the visibility regions are in every case larger when the former one is used. According to Fig. 2 and Table II, the ranges of upgoing/downgoing event numbers, $N_{\text{KT}}^{\text{up/dn}}$, that IC80 will be able to detect in the interval $10^5 - 10^8$ GeV, after five years

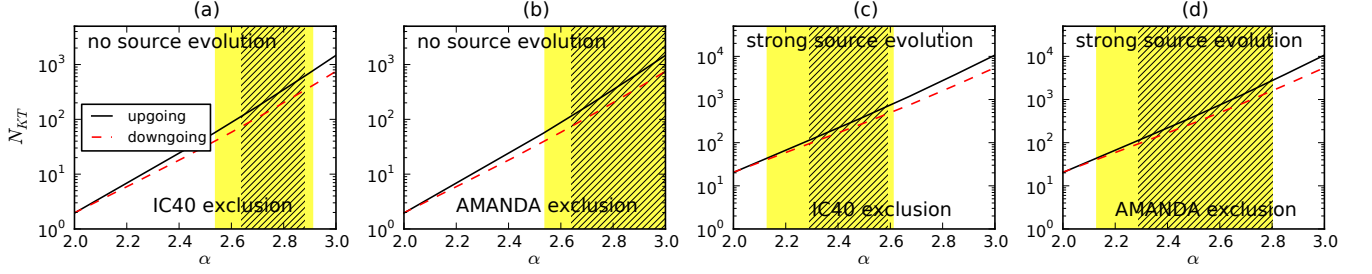


FIG. 2: Integrated number of ν_μ , between 10^5 GeV and 10^8 GeV, expected at IceCube, after $T = 5$ years of exposure, under the assumption of the KT production model. Plots (a) and (b) assume no source evolution, while plots (c) and (d) assume strong source evolution. Upgoing-neutrino event numbers are shown as solid (black) lines, while downgoing event numbers are shown as dashed (red) lines. In plots (a) and (c), the yellow-coloured band is the region of values of α that lies above the IC80PS sensitivity and below the IC40NS upper bound for downgoing neutrinos, while the hatched region is the corresponding one for upgoing neutrinos (see Table II). In plots (b) and (d), the upper bound is the AMANDA bound.

of exposure, are:

$$114 \leq N_{KT}^{\text{up}} \leq 613 (1980) , \quad 41 \leq N_{KT}^{\text{dn}} \leq 411 (990) , \quad (42)$$

assuming no source evolution and using the IC40 (AMANDA) upper bound, and

$$113 \leq N_{KT}^{\text{up}} \leq 697 (2736) , \quad 41 \leq N_{KT}^{\text{dn}} \leq 522 (1589) , \quad (43)$$

assuming strong source evolution.

From these plots, as well as from Table II, we can extract, for each of the two assumptions on source evolution, the minimum value of α to which IC80 will be sensitive, and the maximum allowed value of α , according to either the AMANDA or IC40 visibility criterion. The minimum value of α accessible by IC80 is fixed by the IC80PS sensitivity, and will be the lower one between the sensitivities for upgoing and downgoing neutrinos; under both assumptions on source evolution, the lower α occurs for the latter sample: 2.54 assuming no source evolution and 2.13 assuming strong source evolution. For the AMANDA criterion, the upper limit on α for both the upgoing and downgoing samples at IC80 is the AMANDA-upgoing bound: 3.04 and 2.80, assuming no source evolution and strong source evolution, respectively. Under the IC40 criterion, the upper limit on α is the more restrictive value between the upgoing and downgoing samples, which is in every case the former one: 2.88 for no source evolution and 2.59 for strong source evolution. The ranges of α that IC80 will be able to probe are therefore:

$$2.54 \leq \alpha \leq 2.88 (3.04) , \quad (44)$$

assuming no source evolution and the IC40NS (AMANDA) upper bound, and

$$2.13 \leq \alpha \leq 2.59 (2.80) , \quad (45)$$

assuming strong source evolution. Thus, the KT model with no source evolution is allowed for higher values of α than the model with strong source evolution. This is due to the fact that the KT flux grows with α , and to the fact that the event yield associated with the assumption of strong source evolution is up to an order of magnitude higher than the yield with no source evolution, so that lower values of α are needed to keep the former below the IC40NS or AMANDA event-number upper bounds.

According to Eqs. (44) and (45) the value of $\alpha = 2.7$ that is obtained from fits to cosmic-ray data would still be allowed under the AMANDA visibility criterion, regardless of the choice of source evolution, and under the IC40 visibility criterion assuming no source evolution. Hence, if the IceCube Collaboration officially reports an upper bound using the IC40 data that is close to our estimated bound and if $\alpha = 2.7$ is in fact the true value of the cosmic-ray spectral index, then the KT model with strong source evolution would be discarded as a possible explanation of the AGN neutrino flux.

The bounds on α in Eqs. (44) and (45) can be translated into bounds on the KT flux. Using Eqs. (22) and (23), we find that, between 10^5 GeV and 10^8 GeV,

$$3.11 \times 10^{-11} E_\nu^{-1.54} \leq \frac{\phi_{\nu_\mu}^{\text{diff,KT}}}{\min(1, E_\nu/E_{\nu,\text{br}})} \frac{1}{\text{GeV}^{-1} \text{ cm}^{-2} \text{ s}^{-1} \text{ sr}^{-1}} \leq 5.28 \times 10^{-8} E_\nu^{-1.88} (1.73 \times 10^{-6} E_\nu^{-2.04}) , \quad (46)$$

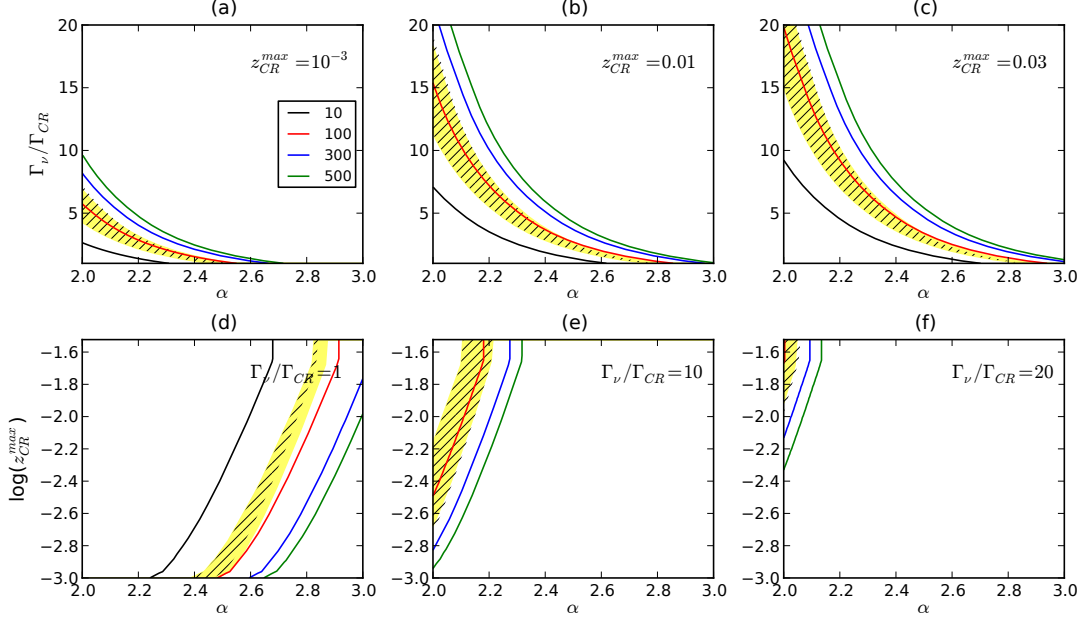


FIG. 3: Variation of the integrated number of downgoing neutrinos expected in the range $10^5 \leq E_\nu/\text{GeV} \leq 10^8$ from the BB model after $T = 5$ years of exposure at the IceCube-80 detector. In (a), (b), and (c), the value of $z_{\text{CR}}^{\text{max}}$ has been fixed, respectively, at the representative values of 10^{-3} , 0.01, and 0.03, while α and $\Gamma_\nu/\Gamma_{\text{CR}}$ have been allowed to vary. Likewise, in (d), (e), and (f), $\Gamma_\nu/\Gamma_{\text{CR}}$ has been fixed at 1, 10, and 20, respectively, while α and $z_{\text{CR}}^{\text{max}}$ have been varied. The solid lines are isocontours of number of events: 10 (black), 100 (red), 300 (blue), and 500 (green). The region coloured yellow is the parameter region where the event-number predictions lie above the IC80PS sensitivity and below the IC40NS upper bound, i.e., the IC40 visibility region. Similarly, the hatched region is where the predictions lie above the IC80PS sensitivity and below the AMANDA upper bound, i.e., the AMANDA visibility region.

assuming no source evolution and the IC40NS (AMANDA) upper bound, and

$$3.80 \times 10^{-14} E_\nu^{-1.13} \leq \frac{\phi_{\nu_\mu}^{\text{diff,KT}}}{\min(1, E_\nu/E_{\nu,\text{br}}) \text{ GeV}^{-1} \text{ cm}^{-2} \text{ s}^{-1} \text{ sr}^{-1}} \leq 7.95 \times 10^{-10} E_\nu^{-1.59} (7.27 \times 10^{-8} E_\nu^{-1.80}) , \quad (47)$$

assuming strong source evolution.

B. BB event-rate expectations at IceCube-80

As to the BB flux model, Figures 3 and 4 show isocontours of the expected integrated number of muon-neutrinos at the IC80 detector, in the $\Gamma_\nu/\Gamma_{\text{CR}}-\alpha$ plane, for fixed values of $z_{\text{CR}}^{\text{max}} = 10^{-3}$ (plots (a)), 0.01 (plots (b)), and 0.03 (plots (c)), and in the $z_{\text{CR}}^{\text{max}}-\alpha$ plane, for fixed values of $\Gamma_\nu/\Gamma_{\text{CR}} = 1$ (plots (d)), 10 (plots (e)), and 20 (plots (f)). Figs. 3 and 4 correspond, respectively, to the downgoing and upgoing samples. The BB normalisation constant, according to Eq. (36), decreases with $z_{\text{CR}}^{\text{max}}$ and increases with $\Gamma_\nu/\Gamma_{\text{CR}}$. The number of events associated to the BB flux, therefore, behaves in the same manner, and this is seen in Figs. 3 and 4. In each plot, as we have mentioned before, the IC40 visibility region is coloured yellow and lies between the IC80PS sensitivity (left border) and the IC40NS upper bound (right border). The AMANDA visibility region, on the other hand, is represented by the hatched region in every plot, and its right border is fixed instead by the AMANDA bound.

Besides the observed narrowness of the visibility regions, there are two main features that we can note in both the downgoing and upgoing samples. The first is that, if the value of $z_{\text{CR}}^{\text{max}}$ increases, the allowed ranges of α and $\Gamma_\nu/\Gamma_{\text{CR}}$ also increase, with higher values being allowed. The second is that, if the value of $\Gamma_\nu/\Gamma_{\text{CR}}$ increases, the allowed ranges of α and $z_{\text{CR}}^{\text{max}}$ are diminished, with α tending to lower values and $z_{\text{CR}}^{\text{max}}$ to higher ones. These observations can be quantified if we project the visibility regions in each plane onto the horizontal and vertical axes.

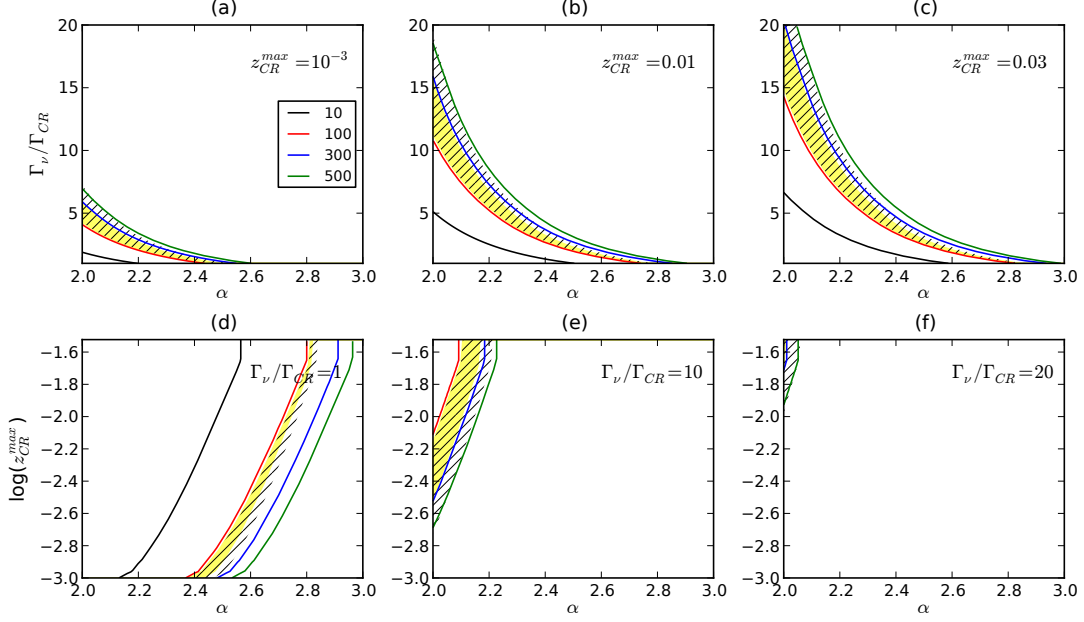


FIG. 4: Same as Fig. 3, but for upgoing neutrinos.

We have built the allowed parameter ranges by selecting the most restrictive and sensitive limits among the AMANDA and IC40 visibility regions of the downgoing and upgoing samples. In every case the upgoing sample and its corresponding IC40 visibility region have been chosen since this choice does a slightly better or equal job than its counterparts. It is interesting to note, however, that for the downgoing sample, when Γ_ν/Γ_{CR} is close to 1, the AMANDA bound restricts the parameter space more than the IC40 bound does. Thus, projecting the IC40 visibility regions in Figs. 4a–c onto the axes, we find that the allowed intervals of α and Γ_ν/Γ_{CR} are given by: $2.0 \leq \alpha \lesssim 2.5$ & $1 \leq \Gamma_\nu/\Gamma_{CR} \lesssim 5.8$ for $z_{CR}^{\max} = 10^{-3}$, $2.0 \leq \alpha \lesssim 2.7$ & $1 \leq \Gamma_\nu/\Gamma_{CR} \lesssim 15$ for $z_{CR}^{\max} = 0.01$, and $2.0 \leq \alpha \lesssim 2.8$ & $1 \leq \Gamma_\nu/\Gamma_{CR} \leq 20.0$ for $z_{CR}^{\max} = 0.03$. Similarly, projecting the visibility regions in Figs. 4d–f, we find for α and z_{CR}^{\max} the following allowed intervals: $2.4 \lesssim \alpha \lesssim 2.81$ & $10^{-3} \lesssim z_{CR}^{\max} \leq 0.03$ for $\Gamma_\nu/\Gamma_{CR} = 1$, and $2.0 \leq \alpha \lesssim 2.18$ & $10^{-2.5} \lesssim z_{CR}^{\max} \leq 0.03$ for $\Gamma_\nu/\Gamma_{CR} = 10$. For $\Gamma_\nu/\Gamma_{CR} = 20$, there is no allowed interval for α and z_{CR}^{\max} .

In light of these results, and considering $\alpha = 2.7$ to be the true value of the cosmic-ray spectral index [46], we see that the BB flux model is clearly excluded for $\Gamma_\nu/\Gamma_{CR} \gtrsim 10$ and for the lowest values of z_{CR}^{\max} , close to 10^{-3} . Whenever $\alpha = 2.7$ is allowed by the BB model, it is only inside a very narrow region of parameter space, around $\Gamma_\nu/\Gamma_{CR} \sim 1$ and $z_{CR}^{\max} \sim 0.03$.

V. COMPARISON BETWEEN THE KT AND BB MODELS USING THE ICECUBE DETECTOR

We have quantified the difference between the predictions put forward by the two models using the quantity

$$\Delta(\alpha, \Gamma_\nu/\Gamma_{CR}, z_{CR}^{\max}) = |N_{BB}(\alpha, \Gamma_\nu/\Gamma_{CR}, z_{CR}^{\max}) - N_{KT}(\alpha)|, \quad (48)$$

and measured it in units of $\sigma(\alpha) \equiv \sqrt{N_{KT}}$. In other words, at every point in parameter space we measure the difference between the number of events predicted by each model, in units of the standard deviation of the KT prediction, assuming for it an uncertainty characteristic of a Gaussian distribution. The higher the value of the number of σ , the greater the difference between the predictions. The comparison between the models, however, is only valid within the regions of parameter space where both models simultaneously lie above the IC80PS sensitivity and below the IC40NS, or AMANDA, upper bound, that is, within the region that results from the intersection of the KT and BB visibility regions. Otherwise, in regions where only one or none of the models are visible (i.e., where the predictions of one or both of them lie below the sensitivity or above the upper bound), the discrimination between them is obvious or is meaningless, respectively. Recalling the results from Section IV, we use the BB visibility region

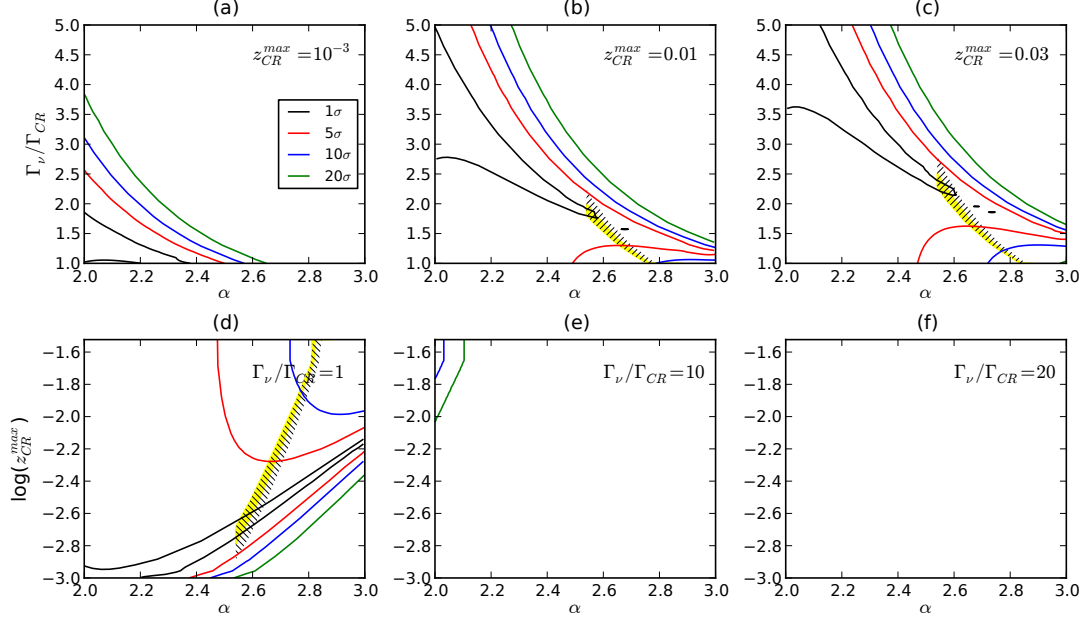


FIG. 5: Separation between the BB and KT models, in terms of $\Delta \equiv |N_{\text{BB}} - N_{\text{KT}}|$, measured in units of $\sigma \equiv \sqrt{N_{\text{KT}}}$ (see text), for downgoing neutrinos with energies in the range $10^5 \leq E_\nu/\text{GeV} \leq 10^8$ and assuming no source evolution for the KT model. The exposure time $T = 5$ years. In (a), (b), and (c), the value of $z_{\text{CR}}^{\text{max}}$ has been fixed, respectively, at the representative values of 10^{-3} , 0.01, and 0.03, while α and $\Gamma_\nu/\Gamma_{\text{CR}}$ have been allowed to vary. Likewise, in (d), (e), and (f), $\Gamma_\nu/\Gamma_{\text{CR}}$ has been fixed at 1, 10, and 20, respectively, while α and $z_{\text{CR}}^{\text{max}}$ have been varied. The solid lines are isocontours of $\Delta = 1\sigma$ (black), 5σ (red), 10σ (blue), and 20σ (green). The region coloured yellow is the parameter region where the event-number predictions of, simultaneously, the KT and BB models lie above the IC80PS sensitivity and below the IC40NS upper bound, i.e., the IC40 visibility region. Similarly, the hatched region is where the predictions of both models lie above the IC80PS sensitivity and below the AMANDA upper bound, i.e., the AMANDA visibility region. Either visibility region represents the region of parameter space where comparison between the two production models is meaningful, according to the two visibility criteria.

for upgoing neutrinos, shown in Fig. 4, and the allowed intervals of α that were obtained for the KT model, Eqs. (44) and (45). This guarantees that the numbers of events predicted by both models lie above the minimum required signal for detection at 5σ from the atmospheric neutrino background, so that the comparison between them is meaningful. In Figures 5–8, we have coloured yellow the region of simultaneous visibility under the IC40 criterion, and hatched the region of simultaneous visibility under the AMANDA criterion. Evidently, since the individual visibility regions of the KT and BB models are larger under the AMANDA visibility criterion than under the IC40 criterion, the regions of simultaneous visibility in Figs. 5–8 are in every case larger under the former.

Thus, Figs. 5–8 show the separation between the models using the integrated number of muon-neutrinos at the full IC80 detector, in the range $E_\nu \in [10^5, 10^8]$ GeV, and assuming $T = 5$ years of exposure. The iso-contours correspond to $\Delta/\sigma = 1$ (black), 5 (red), 10 (blue), and 20 (green), in the plane $\Gamma_\nu/\Gamma_{\text{CR}}-\alpha$, for values of $z_{\text{CR}}^{\text{max}} = 10^{-3}$ (plots (a)), 0.01 (plots (b)), and 0.03 (plots (c)), and in the plane $\log(z_{\text{CR}}^{\text{max}})-\alpha$, for values of $\Gamma_\nu/\Gamma_{\text{CR}} = 1$ (plots (d)), 10 (plots (e)), and 20 (plots (f)).

In all of these figures we see that there is almost no overlap between the KT and BB visibility regions for high values of $\Gamma_\nu/\Gamma_{\text{CR}}$ and that the size of the overlapping regions grows with $z_{\text{CR}}^{\text{max}}$, so that they are largest for $z_{\text{CR}}^{\text{max}} = 0.01$ and 0.03, as shown in plots (b) and (c) of Figs. 5–8. In particular, under the assumption of no source evolution, the regions of simultaneous visibility exist only for low values of $\Gamma_\nu/\Gamma_{\text{CR}}$, between 1 and 3 (see Figs. 5 and 6), while under the assumption of strong source evolution, they exist up to $\Gamma_\nu/\Gamma_{\text{CR}} \approx 15$ (see Figs. 7 and 8). The shape of the regions of simultaneous visibility mainly depends on the type of source evolution used in the KT model, but it is possible to find some differences in the discrimination between models in case you use either the downgoing or upgoing sample, given the same hypothesis for the source evolution. For fixed values of α , $\Gamma_\nu/\Gamma_{\text{CR}}$, and $z_{\text{CR}}^{\text{max}}$, the separation between the models is in general higher when the upgoing neutrino sample is used. But there are also some points in parameter space that may have a higher separation associated to them using the downgoing sample. For instance,

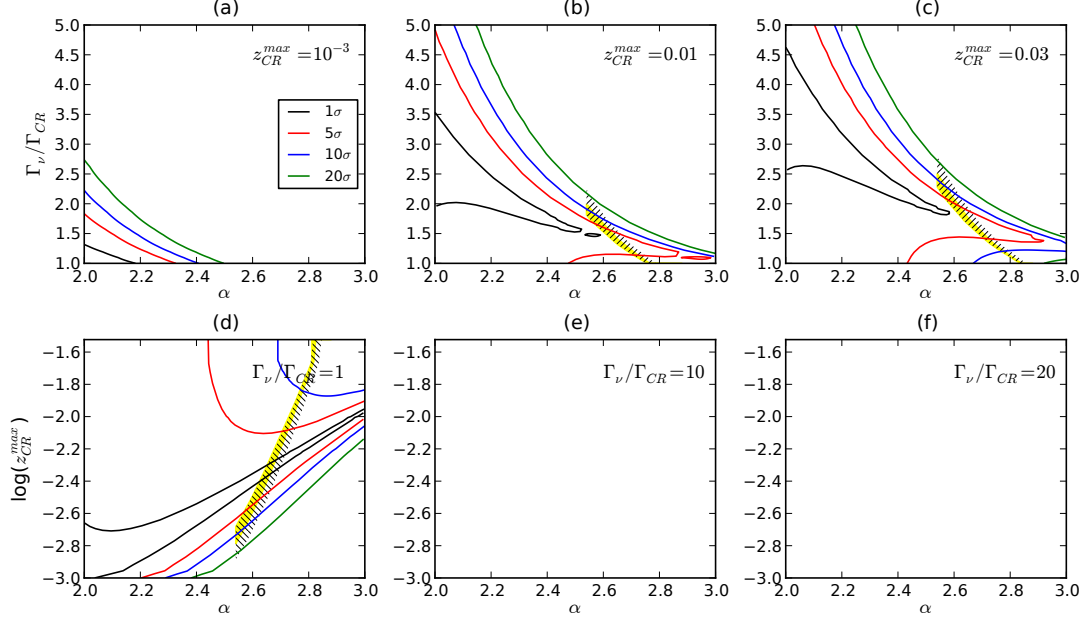


FIG. 6: Same as Fig. 5, but for upgoing neutrinos, assuming no source evolution for the KT model.

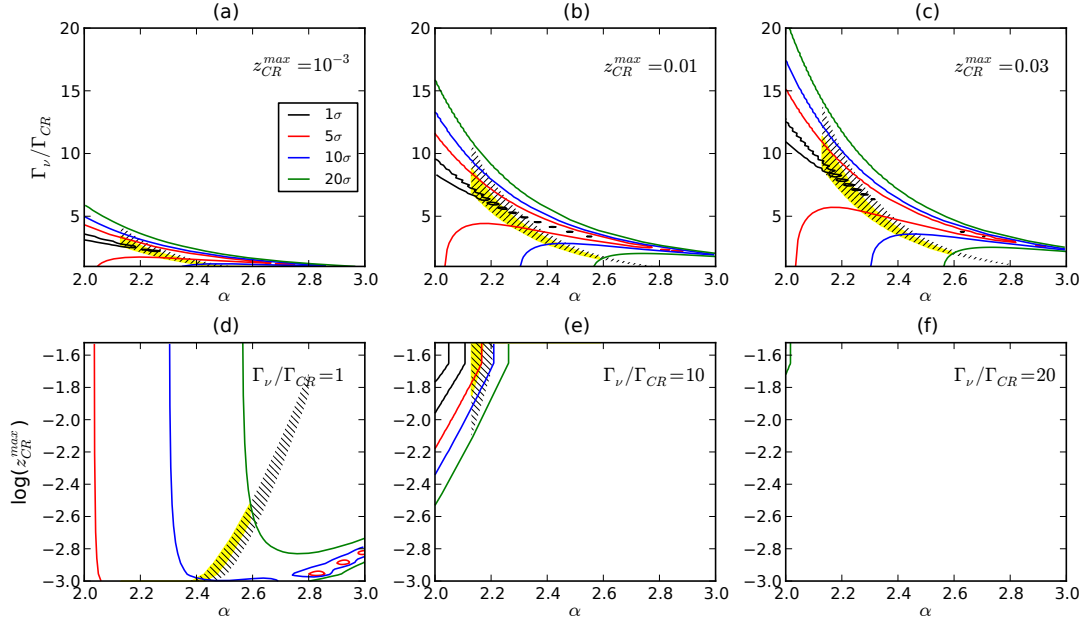


FIG. 7: Same as Fig. 5, but for downgoing neutrinos, assuming strong source evolution for the KT model.

for $\Gamma_\nu/\Gamma_{CR} = 1$ and using the downgoing sample, Fig. 5d shows that the point $(\alpha, \log(z_{CR}^{max})) = (2.65, -2.4)$ has a separation between 1σ and 5σ , whereas, using the upgoing sample, in Fig. 6d, the same point has a separation lower than 1σ .

From Figs. 5 and 6, we see that, within the IC40 visibility region, assuming no source evolution, the two models

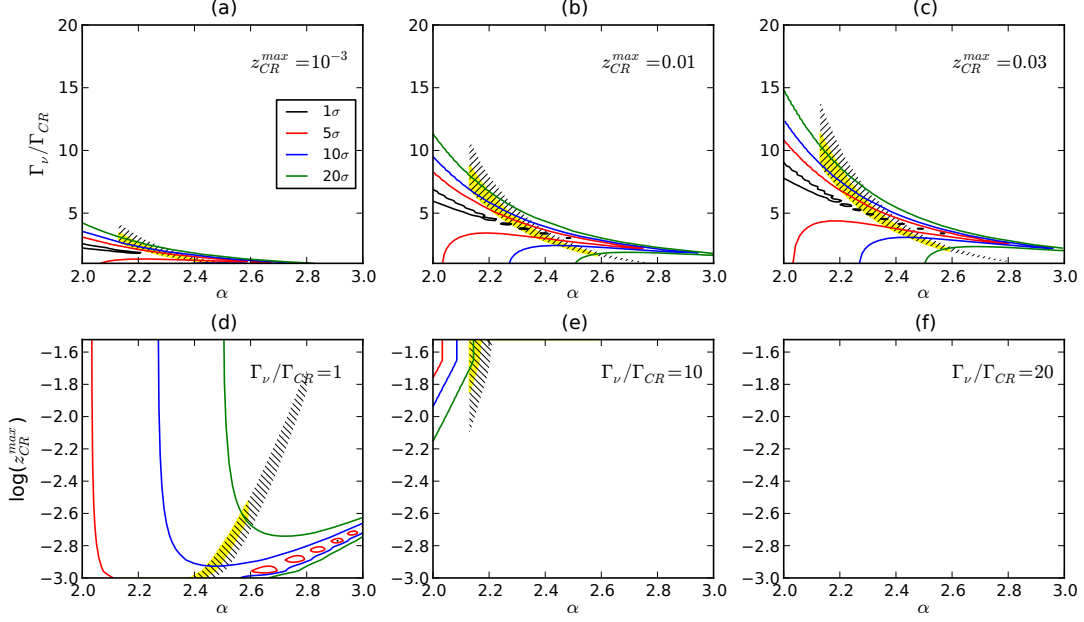


FIG. 8: Same as Fig. 5, but for upgoing neutrinos, assuming strong source evolution for the KT model.

can be separated in up to 10σ , while, as shown by Figs. 7 and 8, assuming strong source evolution, they can reach separations beyond 20σ . On the other hand, if we take the combined discrimination power of the downgoing and upgoing samples, for each of the assumptions on source evolution, we find that within the IC40 regions where the capacity to discern between models is less than 5σ , Γ_ν/Γ_{CR} and α are between $1.2(4.5)$ – $2.2(7)$ and $2.55(2.15)$ – $2.68(2.3)$, respectively, for no (strong) source evolution, and z_{CR}^{max} lies between 0.01 and 0.03. In all other cases the differences are greater than 5σ . Under the AMANDA visibility criterion, slightly larger separations can be achieved. When α is 2.7, or a value close thereto, and when it is within the regions of IC40 simultaneous visibility, we always have differences between the models greater than 5σ , except when $\Gamma_\nu/\Gamma_{CR} \approx 1$ and $z_{CR}^{max} \approx 10^{-2.2}$, under the assumption of no source evolution and using the upgoing sample.

VI. SUMMARY AND CONCLUSIONS

We have studied the IceCube event rate expectations for two models of AGN diffuse muon-neutrino flux proposed in the literature, one by Koers & Tinyakov (KT) [11] and another by Becker & Biermann (BB) [12], both of which take into account the apparent correlation, reported by the Pierre Auger Collaboration, between the incoming directions of the highest-energy ($E > 57$ EeV) cosmic rays and the positions of known AGN. In doing this, we have assumed that the ultra-high-energy (UHE) AGN neutrino flux makes up all of the UHE astrophysical neutrino flux. Both models propose a flux with the shape of a power law, i.e., proportional to $E_\nu^{-\alpha}$, resulting from shock acceleration. In this analysis, we have taken the spectral index, α , as well as two other parameters associated to the BB model, namely, the ratio of relativistic boost factors of neutrinos and cosmic rays, Γ_ν/Γ_{CR} , and the redshift of the most distant AGN that contributes to the diffuse cosmic-ray flux, z_{CR}^{max} , as free parameters, and varied their values within the following intervals: $2 \leq \alpha \leq 3$, $1 \leq \Gamma_\nu/\Gamma_{CR} \leq 20$, and $10^{-3} \leq z_{CR}^{max} \leq 0.03$. On top of that, we have explored the KT model under two assumptions regarding the evolution of the density of the neutrino sources: either they do not evolve with redshift, or they evolve strongly with redshift, following the star formation rate. Event rates calculated using the latter assumption are up to an order of magnitude higher than the ones calculated using the former one.

For each point $(\alpha, \Gamma_\nu/\Gamma_{CR}, z_{CR}^{max})$ in parameter space, we have calculated for both models the associated integrated number of muon-neutrinos, between 10^5 GeV and 10^8 GeV, that is expected after five years of exposure of the full 80-string IceCube neutrino detector (IC80). In order to determine the allowed, and observable, regions of parameter space, we have tested two different upper bounds: one, the upper bound on the neutrino flux already reported by the AMANDA Collaboration, and the other, an estimated upper bound that we have set, under the assumption that no

signal is found in the yet-unreported IC40 data. The lower bound, on the other hand, is fixed by the projected IC80 five-year sensitivity. With this we have defined “regions of visibility” in parameter space as those regions inside which the event-rate predictions lie above the IC80 projected sensitivity and below the reported AMANDA upper bound or, alternatively, below the estimated IC40 upper bound.

For a given flux model and fixed values of the model parameters, the number of upgoing muon-neutrinos is always higher than that of downgoing neutrinos. Since downgoing and upgoing neutrino event rates are calculated in different manners (see Appendix A), however, this difference does not imply that the upgoing sample is capable of achieving a better sensitivity to the parameters. In fact, for the KT model, while the upgoing sample does set the tightest upper bounds on α , a greater sensitivity is achieved by the downgoing sample. Also, since the estimated IC40 upper bound is stronger than the reported AMANDA upper bound, the former restricts the allowed parameter space more than the latter.

In the event that the IceCube Collaboration, using the IC40 data, reports an upper bound (i.e., a negative signal) equal or close to the one estimated by us in the present work, it would be possible to confine the spectral index of the KT model within the range $2.54 \leq \alpha \leq 2.88$ (3.04), under the assumption of no source evolution and using the IC40 (AMANDA) upper bound, or $2.13 \leq \alpha \leq 2.59$ (2.80), under the assumption of strong source evolution. For the KT model, it is straightforward to translate these bounds on α into bounds on the flux, and we have done so in Eqs. (46) and (47).

For the BB model, we found that only the values of $\Gamma_\nu/\Gamma_{\text{CR}} \approx 20$ are not contained within the visibility regions, and that this occurs for the upgoing sample using the IC40 upper bound. The highest values, close to 20, are only allowed within small regions, with $\alpha \lesssim 2.1$ and $z_{\text{CR}}^{\text{max}} \approx 0.03$. The spectral index can take on values within the interval $2 \leq \alpha \leq 2.81$, though the highest values are accessible only with $z_{\text{CR}}^{\text{max}} = 0.01$ to 0.03 . For values of $\Gamma_\nu/\Gamma_{\text{CR}} \sim 1$, the allowed intervals are $2.4 \lesssim \alpha \lesssim 2.81$ and $10^{-3} \leq z_{\text{CR}}^{\text{max}} \leq 0.03$, but as $\Gamma_\nu/\Gamma_{\text{CR}}$ rises, both intervals are reduced until $\Gamma_\nu/\Gamma_{\text{CR}} = 20$, where they have almost disappeared.

Using combined cosmic-ray data [46], the preferred value of α has been set at 2.7. We have found that, if the AMANDA upper bound is used, this value is allowed in the KT model, regardless of the assumption on source evolution. If our estimated IC40 upper bound is used instead, $\alpha = 2.7$ is allowed only under the assumption of no source evolution. On account of this, the KT model with strong source evolution could be discarded if the IC40 upper bound is confirmed with a value close to or lower than the one we have projected. On the other hand, for the BB model, the value $\alpha = 2.7$ is allowed under both the IC40 and AMANDA visibility criteria, though only within very narrow intervals of $\Gamma_\nu/\Gamma_{\text{CR}}$ and $z_{\text{CR}}^{\text{max}}$. This value of α is only allowed for $\Gamma_\nu/\Gamma_{\text{CR}} \lesssim 2$ and for the highest values of $z_{\text{CR}}^{\text{max}}$, between 0.01 and 0.03. Therefore, if $\alpha = 2.7$ is the true value of the spectral index, then the BB model will be discarded except for low values of $\Gamma_\nu/\Gamma_{\text{CR}}$ and high values of $z_{\text{CR}}^{\text{max}}$.

Finally, in the event that an UHE neutrino signal is detected after five years of running the full IceCube array, and assuming that it was produced solely by the neutrino flux from AGN, we have explored the detector’s capability to distinguish between the KT model, with strong and no source evolution, and the BB model, i.e., to determine which one of the two models would correctly describe the detected UHE neutrino data. In order to do this, we have defined a measure of the separation between the models as $\Delta(\alpha, \Gamma_\nu/\Gamma_{\text{CR}}, z_{\text{CR}}^{\text{max}}) \equiv |N_{\text{BB}}(\alpha, \Gamma_\nu/\Gamma_{\text{CR}}, z_{\text{CR}}^{\text{max}}) - N_{\text{KT}}(\alpha)|$, and calculated the value of Δ , expressed in units of $\sigma(\alpha) \equiv \sqrt{N_{\text{KT}}(\alpha)}$, at each point of the parameter space. The comparison between the flux models, however, is meaningful only in those regions of the parameter space where both models simultaneously lie inside their respective visibility regions, i.e., where both models predict event rates that lie 5σ above the atmospheric muon-neutrino rates. In general, these “regions of simultaneous visibility” turn out to be thin strips in parameter space which exist mainly at large values of $z_{\text{CR}}^{\text{max}}$, between 0.01 and 0.03, and that practically disappear at values of $\Gamma_\nu/\Gamma_{\text{CR}} \geq 10$. For no source evolution, at $z_{\text{CR}}^{\text{max}} = 0.03$ the regions of simultaneous visibility exist only at low values of $\Gamma_\nu/\Gamma_{\text{CR}}$, between 1 and 3, while for strong source evolution, they exist up to $\Gamma_\nu/\Gamma_{\text{CR}} = 15$. With regard to the degree of the separation between models we note that the only regions where the separation is lower than 5σ occur at $z_{\text{CR}}^{\text{max}}$ between 0.01 and 0.03, for $\Gamma_\nu/\Gamma_{\text{CR}}$ and α in the intervals 1.2(4.5)–2.2(7) and 2.55(2.15)–2.68(2.3), respectively, for no (strong) source evolution. In all other cases, the distinction between the models is well determined. In the particular case of $\alpha = 2.7$, and values close thereto, the discrimination between the models is in general equal to or better than 5σ .

We have thus shown, firstly, that, after five years of running, the completed IceCube array could be sensitive to both the KT and BB fluxes, though in some cases only if the model parameters lie within very narrow regions of parameter space; and, secondly, that the detector is potentially able to establish which one of the two models is the best description of the UHE diffuse AGN neutrino flux. If no signal is detected after five years of running, however, a tighter upper bound on the neutrino flux will be set, and the regions of parameter space within which the models are able to account for the diffuse neutrino flux will be further reduced.

Acknowledgments

This work was supported by grants from the Dirección Académica de Investigación of the Pontificia Universidad Católica del Perú (projects DAI-4075 and DAI-L009). The authors would like to thank the Dirección de Informática Académica for providing distributed computing support through the LEGION system and Edith Castillo for her collaboration in the early stages of the work.

Appendix A: Neutrino detection at IceCube

We have calculated the predicted number of upgoing and downgoing muon-neutrinos detected at IceCube using the method presented in reference [11]. In general, the integrated number of upgoing (up) or downgoing (dn) muon-neutrinos at a Čerenkov detector due to a diffuse flux of muon-neutrinos, $\phi_{\nu_\mu}^{\text{diff}}$, with energies between E_ν^{min} and E_ν^{max} , is calculated as

$$N_{\nu,\text{up/dn}} = T\Omega \int_{E_\nu^{\text{min}}}^{E_\nu^{\text{max}}} dE_\nu \phi_{\nu_\mu}^{\text{diff}}(E_\nu) A_{\nu,\text{eff}}^{\text{up/dn}}(E_\nu) , \quad (\text{A1})$$

where T is the detector's exposure time; Ω , the detector's opening solid angle; E_ν , the neutrino energy; $\phi_{\nu_\mu}^{\text{diff}}$ is either the KT or BB diffuse AGN neutrino flux (or, in order to calculate the background signal, the atmospheric ν_μ flux); and $A_{\nu,\text{eff}}^{\text{up/dn}}$ is the neutrino effective area.

Note that the six extra DeepCore strings increase the neutrino effective area only in the range $10 \leq E_\nu/\text{GeV} \leq 10^3$ [47]. Above 10^3 GeV, the IceCube effective area is determined solely by the remaining 80 strings.

1. Upgoing ν_μ detection rate at IceCube

For upgoing neutrinos, the effective neutrino area takes the form

$$A_{\nu,\text{eff}}^{\text{up}}(E_\nu) = S(E_\nu) P_\mu(E_\mu) A_{\mu,\text{eff}}^{\text{up}}(E_\mu) \quad (\text{A2})$$

where S is the shadowing factor, which takes into account neutrino interactions within the Earth; P_μ , the probability that the neutrino-spawned muon reaches the detector with energy greater than the threshold energy E_μ^{min} required to be detected; and $A_{\mu,\text{eff}}$, the detector's effective area for muons. We will explain each term in Eq. (A2) in what follows.

The probability of muon detection can be written as [11]

$$P_\mu(E_\mu) = 1 - \exp(-N_{\text{Av}} \sigma_{\nu N}^{\text{CC}}(E_\nu) R_\mu(E_\mu)) , \quad (\text{A3})$$

where $N_{\text{Av}} = 6.022 \times 10^{23} \text{ mol}^{-1} = 6.022 \times 10^{23} \text{ cm}^{-3}$ (w.e., water equivalent) is Avogadro's constant; $\sigma_{\nu N}^{\text{CC}}$ is the charged-current neutrino-nucleon cross section, taken from [48] (which uses CTEQ4 data); and R_μ is the muon range within which the muon energy reaches the threshold energy E_μ^{min} , which can be expressed as

$$R_\mu(E_\mu) = \frac{1}{b} \ln \left(\frac{a + bE_\mu}{a + bE_\mu^{\text{min}}} \right) , \quad (\text{A4})$$

with $a = 2.0 \times 10^{-3} \text{ GeV cm}^{-1}$ (w.e.) accounting for ionisation losses and $b = 3.9 \times 10^{-6} \text{ cm}^{-1}$ (w.e.) accounting for radiation losses. The relation between neutrino and muon energy is obtained by assuming single-muon production in each neutrino interaction, which leads to $E_\mu = y_{\text{CC}}(E_\nu) E_\nu$, with y_{CC} the mean charged-current inelasticity parameter tabulated in [48].

The shadowing factor, S , is defined in terms of $P_\nu(E_\nu, \theta)$, the probability that a neutrino arriving at Earth with nadir angle θ (the North Pole is located at $\theta = 0^\circ$) and interacting with Earth matter, reaches the detector. We use [11]

$$S(E_\nu) = \frac{1}{1 - \cos(\theta_{\text{max}})} \int_0^{\theta_{\text{max}}} d\theta \sin(\theta) P_\nu(E_\nu, \theta) , \quad (\text{A5})$$

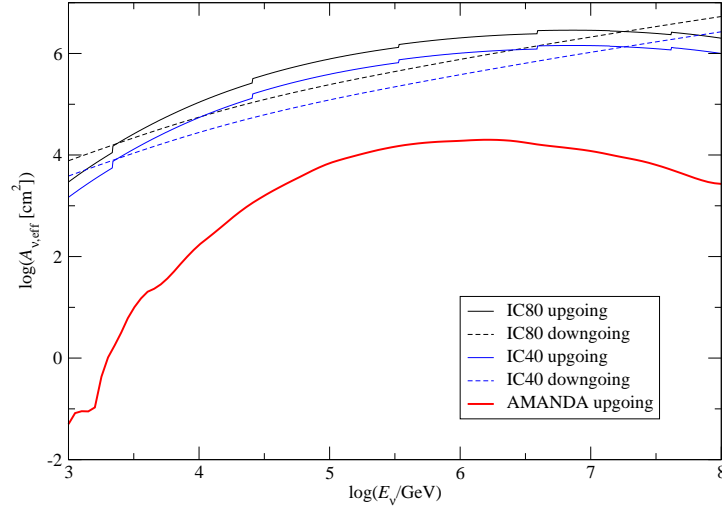


FIG. 9: Angle-averaged neutrino effective areas, as functions of the neutrino energy, for the IC80, IC40, and AMANDA detectors. The IC40 effective area is one half the IC80 area, while the AMANDA effective area is a factor of 100 lower than the IC80 area.

where θ_{\max} is the detector's maximum viewing angle, which we have taken to be $\theta_{\max} = 85^\circ$, as in [11]. Thus, the detector's opening angle is

$$\Omega = \int_0^{2\pi} d\phi \int_0^{\theta_{\max}} \sin(\theta) d\theta = 2\pi [1 - \cos(\theta_{\max})] \approx 5.736 \text{ sr} . \quad (\text{A6})$$

The neutrino survival probability can be written as

$$P_\nu(E_\nu, \theta) = \exp \left(-N_{\text{Av}} \sigma_{\nu N}^{\text{tot}}(E_\nu) \int_0^{L(\theta)} \rho(r) dl \right) , \quad (\text{A7})$$

where $\sigma_{\nu N}^{\text{tot}}$ is the total (charged- plus neutral-current) neutrino-nucleon cross section, tabulated in [48]; $\rho(r)$ is the Earth's density profile given by the Preliminary Reference Earth Model [49], parametrised by the radial coordinate $r = \sqrt{l^2 + r_E^2 - 2lr_E \cos(\theta)}$, with $r_E = 6371$ km the Earth radius; and $L(\theta) = 2r_E \cos(\theta)$ is the distance that a neutrino traversing the Earth at angle θ propagates.

Lastly, for IceCube's upgoing muon effective area, $A_{\mu, \text{up}}^{\text{up}}$, we have used the curve corresponding to level-2 cuts in Figure 5 of Ref. [43], which is the effective area averaged over the northern hemisphere, and dependent only on the incoming muon energy, E_μ . Figure 9 shows that the IC40 neutrino effective area is one half the IC80 effective area, while the AMANDA neutrino effective area was a factor of 100 lower than IC80 area.

2. Downgoing ν_μ detection rate at IceCube

Downgoing neutrinos suffer little interaction before reaching the detector, so that $P_\nu \simeq 1$ and $P_\mu \simeq N_{\text{Av}} \sigma_{\nu N}^{\text{CC}} \min(R_\mu, R_d)$, where $R_d = 2 \times 10^5$ cm is the detector depth. Note that for neutrino energies between 10^5 GeV and 10^{11} GeV, $R_d < R_\mu$. For downgoing muons, the effective area at IceCube can be approximated by a constant-valued $A_{\mu, \text{eff}}^{\text{dn}} = 10^{10}$ cm². Hence, the neutrino effective area for downgoing neutrinos is estimated as

$$A_{\nu, \text{eff}}^{\text{dn}}(E_\nu) = R_d N_{\text{Av}} \sigma_{\nu N}^{\text{CC}}(E_\nu) A_{\mu, \text{eff}}^{\text{dn}} . \quad (\text{A8})$$

- [2] J. Aird *et al.*, arXiv:0910.1141 [astro-ph.CO].
- [3] B. McKernan, K. E. S. Ford and C. Reynolds, arXiv:1005.4907 [astro-ph.CO].
- [4] C. M. Gaskell, arXiv:0908.0328 [astro-ph.CO].
- [5] K. Ptitsyna and S. V. Troitsky, arXiv:0808.0367 [astro-ph].
- [6] M. Kachelriess, arXiv:0801.4376 [astro-ph].
- [7] J. Abraham *et al.* [Pierre Auger Collaboration], *Astropart. Phys.* **29**, 188 (2008) [Erratum-ibid. **30**, 45 (2008)] [arXiv:0712.2843 [astro-ph]].
- [8] M. P. Véron-Cetty and P. Véron *A & A* **455**, 773 (2006).
- [9] H. B. J. Koers and P. Tinyakov, *JCAP* **0904**, 003 (2009) [arXiv:0812.0860 [astro-ph]].
- [10] G. R. Farrar, I. Zaw and A. A. Berlind, arXiv:0904.4277 [astro-ph.HE].
- [11] H. B. J. Koers and P. Tinyakov, *Phys. Rev. D* **78**, 083009 (2008) [arXiv:0802.2403 [astro-ph]].
- [12] J. K. Becker and P. L. Biermann, *Astropart. Phys.* **31**, 138 (2009) [arXiv:0805.1498 [astro-ph]].
- [13] F. Aharonian [HESS Collaboration], arXiv:0711.3196 [astro-ph].
- [14] F. Aharonian [HESS Collaboration], *Astrophys. J. Lett.* **695**, L40 (2009) arXiv:0903.1582 [astro-ph.CO].
- [15] VERITAS Collaboration, H.E.S.S. Collaboration and MAGIC Collaboration, *Science* **325**, 444 (2009) [arXiv:0908.0511 [astro-ph.HE]].
- [16] J. Albert *et al.* [MAGIC Collaboration], *Astrophys. J.* **654**, L119 (2007) [arXiv:astro-ph/0606161].
- [17] J. Albert *et al.* [MAGIC Collaboration], *Astrophys. J.* **663**, 125 (2007) [arXiv:astro-ph/0603478].
- [18] J. Albert *et al.* [MAGIC Collaboration], *Astrophys. J.* **667**, L21 (2007) [arXiv:0706.4435 [astro-ph]].
- [19] H. Anderhub, arXiv:0907.2386 [astro-ph.CO].
- [20] V. Acciari *et al.* [VERITAS Collaboration], arXiv:0812.0978 [astro-ph].
- [21] V. A. Acciari *et al.* [VERITAS Collaboration], *AIP Conf. Proc.* **1085**, 565 (2009) [arXiv:0901.4561 [astro-ph.HE]].
- [22] V. A. Acciari *et al.* [VERITAS Collaboration], *Astrophys. J.* **693**, L104 (2009) [arXiv:0901.4527 [astro-ph.HE]].
- [23] D. A. Williams [Milagro Collaboration], *AIP Conf. Proc.* **745**, 499 (2005).
- [24] J. A. Goodman [Milagro Collaboration], *AIP Conf. Proc.* **917**, 202 (2007).
- [25] F. Halzen, *AIP Conf. Proc.* **1182**, 14 (2009) [arXiv:0906.3470 [astro-ph.HE]].
- [26] X. W. Xu [IceCube Collaboration], *Nucl. Phys. Proc. Suppl.* **175-176**, 401 (2008).
- [27] F. Halzen, *J. Phys. Conf. Ser.* **171**, 012014 (2009) [arXiv:0901.4722 [astro-ph.HE]].
- [28] A. M. Brown, *AIP Conf. Proc.* **1178**, 76 (2009) [arXiv:0908.1035 [astro-ph.HE]].
- [29] P. Lipari, M. Lusignoli and D. Meloni, *Phys. Rev. D* **75**, 123005 (2007) [arXiv:0704.0718 [astro-ph]].
- [30] H. Athar, C. S. Kim and J. Lee, *Mod. Phys. Lett. A* **21**, 1049 (2006) [arXiv:hep-ph/0505017].
- [31] J. F. Beacom, N. F. Bell, D. Hooper, S. Pakvasa and T. J. Weiler, *Phys. Rev. D* **68**, 093005 (2003) [Erratum-ibid. **D 72**, 019901 (2005)] [arXiv:hep-ph/0307025].
- [32] A. Bhattacharya, S. Choubey, R. Gandhi and A. Watanabe, arXiv:1006.3082 [hep-ph].
- [33] G. Barenboim and C. Quigg, *Phys. Rev. D* **67**, 073024 (2003) [arXiv:hep-ph/0301220].
- [34] J. L. Bazo, M. Bustamante, A. M. Gago and O. G. Miranda, *Int. J. Mod. Phys. A* **24**, 5819 (2009) [arXiv:0907.1979 [hep-ph]].
- [35] M. Bustamante, A. M. Gago and C. Pena-Garay, *JHEP* **1004**, 066 (2010) [arXiv:1001.4878 [hep-ph]].
- [36] B. J. Boyle and R. Terlevich, arXiv:astro-ph/9710134.
- [37] A. Cuoco and S. Hannestad, *Phys. Rev. D* **78**, 023007 (2008) [arXiv:0712.1830 [astro-ph]].
- [38] K. Mannheim, R. J. Protheroe and J. P. Rachen, *Phys. Rev. D* **63**, 023003 (2001) [arXiv:astro-ph/9812398].
- [39] C. J. Willott, S. Rawlings, K. M. Blundell, M. Lacy and S. A. Eales, *Mon. Not. Roy. Astron. Soc.* **322**, 536 (2001) [arXiv:astro-ph/0010419].
- [40] J. S. Dunlop and J. A. Peacock, *Mon. Not. Roy. Astron. Soc.* **247**, 19 (1990).
- [41] J. K. Becker, private communication (2009).
- [42] A. Achterberg *et al.* [IceCube Collaboration], *Phys. Rev. D* **76**, 042008 (2007) [Erratum-ibid. **D 77**, 089904 (2008)] [arXiv:0705.1315 [astro-ph]].
- [43] J. Ahrens *et al.* [IceCube Collaboration], *Astropart. Phys.* **20**, 507 (2004) [arXiv:astro-ph/0305196].
- [44] M. L. Costantini and F. Vissani, *Astropart. Phys.* **23**, 477 (2005) [arXiv:astro-ph/0411761].
- [45] S. Grullon, arXiv:1005.4962 [astro-ph.HE].
- [46] V. Berezhinsky, A. Z. Gazizov and S. I. Grigorieva, *Phys. Rev. D* **74**, 043005 (2006) [arXiv:hep-ph/0204357].
- [47] C. Wiebusch [IceCube Collaboration], arXiv:0907.2263 [astro-ph.IM].
- [48] R. Gandhi, C. Quigg, M. H. Reno and I. Sarcevic, *Phys. Rev. D* **58**, 093009 (1998) [arXiv:hep-ph/9807264].
- [49] R. Gandhi, C. Quigg, M. H. Reno and I. Sarcevic, *Astropart. Phys.* **5**, 81 (1996) [arXiv:hep-ph/9512364].